PCT WORLD INTELLECTUAL PROPERTY ORGANIZATION
International Bureau

INTERNATIONAL APPLICATION PUBLISHED UNDER THE PATENT COOPERATION TREATY (PCT)

(51) International Patent Classification 6 : H01M

A2

(11) International Publication Number: **WO 98/15986**

(43) International Publication Date: 16 April 1998 (16.04.98)

(21) International Application Number: PCT/US97/18179

(22) International Filing Date: 6 October 1997 (06.10.97)

(30) Priority Data:
60/028,453 10 October 1996 (10.10.96) US

(71) Applicant: ENECO, INC. [US/US]; 391-B Chipeta Way, Salt Lake City, UT 84108 (US).

(72) Inventor: KUCHEROV, Yan, R.; 5272 Cobble Creek Road #12J, Salt Lake City, UT 84117 (US).

(74) Agent: EVANS, Paul, S.; Eneco, Inc., 391-B Chipeta Way, Salt Lake City, UT 84108 (US).

(81) Designated States: AL, AM, AT, AU, AZ, BA, BB, BG, BR, BY, CA, CH, CN, CU, CZ, DE, DK, EE, ES, FI, GB, GE, GH, HU, ID, IL, IS, JP, KE, KG, KP, KR, KZ, LC, LK, LR, LS, LT, LU, LV, MD, MG, MK, MN, MW, MX, NO, NZ, PL, PT, RO, RU, SD, SE, SG, SI, SK, SL, TJ, TM, TR, TT, UA, UG, UZ, VN, YU, ZW, ARIPO patent (GH, KE, LS, MW, SD, SZ, UG, ZW), Eurasian patent (AM, AZ, BY, KG, KZ, MD, RU, TJ, TM), European patent (AT, BE, CH, DE, DK, ES, FI, FR, GB, GR, IE, IT, LU, MC, NL, PT, SE), OAPI patent (BF, BJ, CF, CG, CI, CM, GA, GN, ML, MR, NE, SN, TD, TG).

Published
Without international search report and to be republished upon receipt of that report.

(54) Title: METHOD AND APPARATUS FOR ENERGY GENERATION

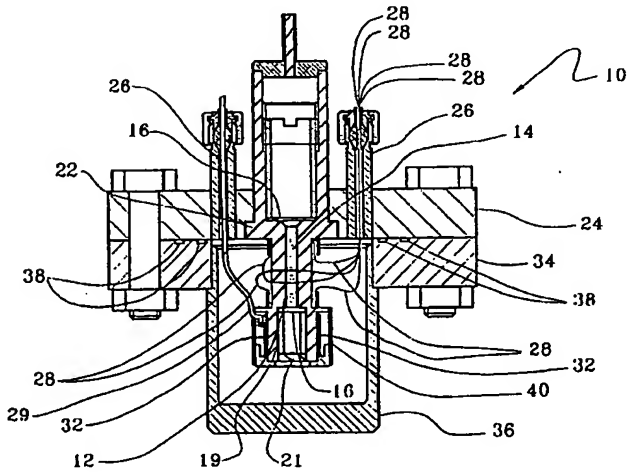

(57) Abstract

A method and apparatus (10, 146) for generating energy, which utilizes a sustained phonon resonance in a lattice with two or more components. The first component (14, 111, 112, 162, 164) comprises elements having nuclei with quadrupole moment. The second component (74) comprises elements having atomic charge less than the first component (14, 111, 112, 162, 164), a different phonon spectrum than the first component (14, 111, 112, 162, 164), and vacancies in the lattice. The phonon resonance within the lattice is sustained at a frequency resonance of 10^{11} to 10^{14} Hz, such that the energy replenishment rate of the phonon resonance is greater than the energy transfer rate to the first component (14, 111, 112, 162, 164). Creating and sustaining a phonon resonance within the lattice may be accomplished by applying a thermal flux, a photon flux, or microwave radiation along the lattice surface.

FOR THE PURPOSES OF INFORMATION ONLY

Codes used to identify States party to the PCT on the front pages of pamphlets publishing international applications under the PCT.

AL	Albania	**ES**	Spain	**LS**	Lesotho	**SI**	Slovenia
AM	Armenia	**FI**	Finland	**LT**	Lithuania	**SK**	Slovakia
AT	Austria	**FR**	France	**LU**	Luxembourg	**SN**	Senegal
AU	Australia	**GA**	Gabon	**LV**	Latvia	**SZ**	Swaziland
AZ	Azerbaijan	**GB**	United Kingdom	**MC**	Monaco	**TD**	Chad
BA	Bosnia and Herzegovina	**GE**	Georgia	**MD**	Republic of Moldova	**TG**	Togo
BB	Barbados	**GH**	Ghana	**MG**	Madagascar	**TJ**	Tajikistan
BE	Belgium	**GN**	Guinea	**MK**	The former Yugoslav Republic of Macedonia	**TM**	Turkmenistan
BF	Burkina Faso	**GR**	Greece			**TR**	Turkey
BG	Bulgaria	**HU**	Hungary	**ML**	Mali	**TT**	Trinidad and Tobago
BJ	Benin	**IE**	Ireland	**MN**	Mongolia	**UA**	Ukraine
BR	Brazil	**IL**	Israel	**MR**	Mauritania	**UG**	Uganda
BY	Belarus	**IS**	Iceland	**MW**	Malawi	**US**	United States of America
CA	Canada	**IT**	Italy	**MX**	Mexico	**UZ**	Uzbekistan
CF	Central African Republic	**JP**	Japan	**NE**	Niger	**VN**	Viet Nam
CG	Congo	**KE**	Kenya	**NL**	Netherlands	**YU**	Yugoslavia
CH	Switzerland	**KG**	Kyrgyzstan	**NO**	Norway	**ZW**	Zimbabwe
CI	Côte d'Ivoire	**KP**	Democratic People's Republic of Korea	**NZ**	New Zealand		
CM	Cameroon			**PL**	Poland		
CN	China	**KR**	Republic of Korea	**PT**	Portugal		
CU	Cuba	**KZ**	Kazakstan	**RO**	Romania		
CZ	Czech Republic	**LC**	Saint Lucia	**RU**	Russian Federation		
DE	Germany	**LI**	Liechtenstein	**SD**	Sudan		
DK	Denmark	**LK**	Sri Lanka	**SE**	Sweden		
EE	Estonia	**LR**	Liberia	**SG**	Singapore		

METHOD AND APPARATUS FOR ENERGY GENERATION

FIELD OF THE INVENTION

This invention relates to methods and apparatus for generating energy by forming a lattice with two or more components having heavy and light elements, and more particularly to such methods and apparatus which utilize a sustained phonon resonance.

BACKGROUND OF THE INVENTION

The present invention improves upon the invention disclosed in my previous U.S. Patent No. 5,632,870 ('870), entitled "Energy Generation Apparatus", by utilizing a sustained phonon resonance to enhance the energy generated. It is presently known that certain metals and alloys have the capability of storing gases in large quantities. The process of loading comprises the dissociation of molecular gas and diffusion into a metal. The process of deloading of a metal includes diffusion and atomic gas recombination on the surface. The net effect of hydrogen loading and deloading can be quite exothermic, as disclosed in U.S. Patent No. 4,599,867, entitled "Hydrogen Storage Cell." The dissociation of a gas into a metal is normally an endothermic process, and the recombination process upon deloading is an exothermic process. When these two processes are separated in time and space, they can be the basis for an efficient heat pump, as disclosed in my '870 patent.

The present invention was developed to fill a need for a device which efficiently generates energy. The invention may be used for energy transfer and storage. The inventor of the present invention has discovered that a sustained phonon resonance within a solid-state lattice of specific heavy and light elements enhances the rate of energy generation over the background art.

SUMMARY OF THE INVENTION

The apparatus and method of this invention constitute an important advance in the art of energy generation, as evidenced by the following objects and advantages realized by the invention.

One object of the present invention is to create a stable phonon resonance.

A further object of the present invention is to maintain a stable, standing phonon resonant wave of sufficient intensity by utilizing the primary resonator harmonic or related harmonics to minimize phonon attenuation.

Additionally, it is an object of the present invention to create the necessary conditions for enhanced energy to be generated using a sustained phonon resonance in a solid-state lattice for specific elements.

Yet another object of the present invention is to create a thermal battery.

Additional objects and advantages of the invention will be apparent from the description which follows, or may be learned by the practice of the invention.

Briefly summarized, the foregoing objects are achieved by an apparatus which comprises a lattice capable of providing a sustained phonon resonance, wherein the lattice comprise a first and second component with the first component from the group of elements comprising Pd, Sm, Eu, Tb, Dy, Au, or combinations thereof; and a second component comprising elements having atomic mass less than the first component, a different phonon spectrum than the first component, vacancies in the lattice; and a means for creating and sustaining a phonon resonance within the lattice having a resonance frequency of 10^{11} to 10^{14} Hz. Creating and sustaining a phonon resonance within the lattice may be accomplished by applying a thermal flux, an optical flux, or microwave radiation along the lattice surface.

BRIEF DESCRIPTION OF DRAWINGS

In order to more fully understand the manner in which the above-recited advantages and objects of the invention are obtained, a more particular description of the invention will be rendered by reference to specific embodiments thereof, which are illustrated in the appended drawings. Understanding that these drawings depict only typical embodiments of the invention and are, therefore, not to be considered limiting of its scope, the presently preferred embodiments and the presently understood best mode of the invention will be described with additional detail through the use of the accompanying drawings in which:

FIG. 1 is a perspective view of an inelastic neutron scattering spectrum for PdH_x (x=0.17; 0.67) of the optical hydrogen vibrations measured with a triple axis

beryllium filter spectrometer. The symbols represent the experimental data for x = 0.17 and x=0.67. The center frequencies of the optical peaks for x = 0.17 and x = 0.67 are v = 15.0 Thz and V = 13.8 Thz, respectively, which incorporates the teachings of the present invention.

FIG. 2 is a graph of a resonator mode intensity behavior in a Pd-H system derived from FIG. 1.

FIG. 3 is a three-dimensional patched graph illustrating a resonant condition in a solid-state lattice.

FIG. 4 is an idealized distribution of atomic layers in a phonon resonator with a planar reflecting surface.

FIG. 5 is a broad band stable phonon resonator.

FIG. 6 is a stack of microwire resonators excited by a thermal gradient.

FIG. 7 is a phonon standing wave structure in a sphere.

FIG. 8 is a phonon standing wave structure in an ellipse.

FIG. 9 is a macroscopic phonon resonator made of spherical particles comprising a two-component material, enclosed in an envelope having a temperature gradient between the two ends.

FIG. 10 is a graph of the result using phonon spectral density normalization $\int_0^\infty I(\omega)d\omega = \int_0^\infty I(\lambda)d\lambda = 1$ on Figure 1.

FIG. 11 illustrates the dipole size, formed by a stable charge vacancy in a solid-

state lattice, dependence on the phonon frequency.

FIG. 12 is a graph showing the calculated phonon mode intensity gain for absolute temperature and the thermal gradient for palladium with an initial temperature of 300K.

FIG. 13 is a cross-sectional view of an embodiment of the present invention, wherein a phonon resonance is created and maintained through application of a thermal gradient.

FIG. 14 is a perspective view of an embodiment of the present invention.

FIG. 15 is a schematic of the vacuum system for the embodiment shown in FIG. 13.

FIG. 16 is a schematic of the gas system for the embodiment shown in FIG. 13.

FIG. 17 is a calibration curve which was measured for two separate heater wires used to create a thermal gradient for the embodiment shown in FIG. 13.

FIGS. 18 and 19 are plots of input power and output power versus time from experiments performed with the embodiment shown in FIG. 13.

FIG. 20 is a plot of the cumulative energy balance from the experiments performed on the embodiment shown in FIG. 13.

FIG. 21 illustrates a wedge-shaped broad-band phonon resonator made of alternating layers of palladium and rhenium.

FIG. 22 illustrates the method in which a wedge-shape structure was achieved by displacing a substrate from the atomic beam center and putting it at an angle to the beam axis.

FIG. 23 is a cross-sectional view of a broad-band phonon resonator shown in Figure 21 in a glow discharge environment.

FIG. 24 is a cross-sectional view of a cathode portion of the glow discharge device shown in Figure 23.

FIG. 25 is a cross-sectional view of the cathode portion of the glow discharge device shown in Figure 23, and incorporating an additional thermal resistance in the form of Cu and Mo discs.

FIG. 26 is a cross-sectional view of a water heater application.

FIG. 27 is a two-component lattice consisting of a light element with mass *m*, vacancy V_4, and a heavy element with mass *M* and Spin S in its nucleus.

FIG. 28 illustrates a nucleus of a heavy element *M*, shown as a quadrupole, sitting near the minimum potential x_o , with its spin S aligned along the x-axis and looking at the xx-component of the electric field tensor created by movements of the sublattice *m*.

DETAILED DESCRIPTION OF THE INVENTION

Two or More Component Lattice

The present invention utilizes a lattice with two or more components capable of providing a sustained phonon resonance. The first component comprises elements having nuclei with a quadrupole moment greater than .001 barn. The second component preferably comprises elements having an atomic mass at least four times lighter than the first one, in order to have significantly different phonon spectra. However, essentially all that is required are elements of the first and second components with different phonon spectra. Moreover, the first component may be in the form of an impurity in another host material, such as impurities in nickel.

A particular concentration of heavy to light elements is not required to create a phonon resonance. However, near stoichiometric compositions are preferred, such as within 5-10% of stoichiometry because of lower phonon attenuation.

For energy generation applications, the first component comprises the elements ^{105}Pd, ^{147,149}Sm, ^{151}Eu, ^{159}Tb, ^{161}Dy, ^{197}Au, or combinations thereof.

For energy storage applications, the first component may comprise the above listed elements for energy generation; however, the preferred elements are isotopes with large quadrupole moments, which include: ^{61}Ni, ^{63,65}Cu, ^{67}Zn, ^{69,71}Ga, ^{75}As, ^{79,81}Br, ^{87}Rb, ^{87}Sr, ^{91}Zr, ^{95,97}Mo, ^{99,101}Ru, ^{105}Pd, ^{135}Ba, ^{141}Pr, ^{145}Nd, ^{147}Sm, ^{155,157}Gd, ^{161}Dy, ^{165}Ho, ^{181}Ta, ^{189}Os, ^{201}Hg, or combinations thereof. Since the energy transfer is probably limited to about 5-10MeV, some of the elements with higher endothermic reactions also can be used for storage applications. Elements such as ^{63,65}Cu have allowed reactions with endothermic energy of more than 18 MeV. ^{61}Ni (-13.8 MeV) can also be used for energy storage.

The second component comprises deuterium, hydrogen, lithium, beryllium, borides, nitrides, oxides, fluorides, chlorides, halides, carbides, or combinations thereof.

One example of a heavy-light element combination in a two-component lattice is hydrides. According to *CRC Handbook of Chemistry and Physics*, 73rd ed. Boca Raton, CRC Press, 1992, pp. II-29 to II-130, a list of stable elements with a large quadrupole moment and forming a hydride lattice includes: ^{43}Ca, ^{45}Sc, ^{47,49}Ti, ^{61}Ni;

^{91}Zr; ^{93}Nb; ^{97}Mo; ^{105}Pd, and elements with atomic numbers 57-80, which includes most of the lantanoides, Hf, Ta, and Re. Ir, Os and Au do not form a hydride lattice under normal conditions, but can form it under any of the well-known hydrogen implantation methods. The largest quadrupole moment among this group occurs with ^{179}Hf, ^{181}Ta, and rare-earth Ho, Ez, Yb, and Lu, being around 3 barns ($3 \cdot 10^{-24}$ cm^2). Most of the elements with atomic charge higher than 85 have asymmetric odd nuclei and thus quadrupole moment. Deuterium also has a small quadrupole moment (0.0028 barn). Light nuclei such as Li, ^{9}Be, $^{10,11}B$, and ^{17}O also have small quadrupole moment.

Consequently, achieving sustained resonant conditions is possible with a variety of components in a combined lattice, though hydrogen, being the lightest of all nuclei, provides for the highest frequencies in its phonon spectrum.

Phonon Resonance

A hydride example is discussed below because of the existence of numerous experimental data. However, the same approach applies to borides, carbides, nitrides, halides, oxides, or lithium alloys or any other heavy/light alloys or compounds defined herein.

A typical spectrum of hydrogen optical phonons in palladium, obtained by inelastic neutron scattering, is shown in Figure 1. (*See* Landolt-Börnstein, *Numerical Data and Functional Relationships in Science and Technology, Group III: Crystal and Solid State Physics*, (1983) Vol. 13b, p. 353). However, the dispersion does not strongly depend on the hydrogen and deuterium concentration. From this figure it can be concluded that the phonon density of states is very low outside the frequency interval from 10^{11} to 10^{14} Hz. This is the region of interest for the present invention. Outside this region, even with amplification provided by a resonator, it is difficult to create a strong phonon mode.

Phonon attenuation can be estimated on the basis of known relationships (*See* Tucker, J.W. et al., *Microwave Ultrasonics in Solid State Physics*, Amsterdam, American Elsevier Publishing Co., 1972, pp. 302-304). Attenuation α [m^{-1}] is described by the relation:

$$\alpha = \frac{1}{L} \ln (I_o/I_L) \quad , \quad (3)$$

where L is the length where attenuation occurs, and I_o and I_L are the acoustic intensities at zero length and length L.

Using data from *Tables of Physical Values*, I.S. Grigoriev Ed., Moscow, Atomizdat, 1991, pp. 156 & 159, a table can be constructed which gives the "e" times attenuation for Ni. Attenuation is different along various crystallographic orientations and is much stronger with polycrystals, when there is a phonon scattering on grain boundaries.

The extrapolated values for attenuation for nickel at 300 K are given in Table 1.

TABLE 1

Phonon Frequency ω, Hz	Attenuation for Ni Single Crystal along <110> α, m^{-1}	Attenuation for Ni polycrystal α, m^{-1}
10^{11}	$1.0 \cdot 10^4$	$1.6 \cdot 10^6$
10^{12}	$1.0 \cdot 10^5$	$1.6 \cdot 10^7$
10^{13}	$1 \cdot 10^6$	$1.6 \cdot 10^8$
10^{14}	$1 \cdot 10^7$	$1.6 \cdot 10^9$

The phonon wavelength is $\lambda = c/\omega$, where c is the speed of sound and ω is the phonon frequency. A resonant condition follows the equation $n \frac{\lambda}{2} = L$, where L is the distance between phonon reflecting surfaces, and n is an integer. The resonance width is $\Delta = \frac{\lambda^2}{2L}$. Table 3 provides the phonon frequencies in Hertz, phonon wavelength λ in meters, and resonance width Δ in meters for Q = 100 (Q is the resonator quality).

TABLE 2

ω_i	λ_i	Δ_i
$2 \cdot 10^{11}$	$1.5 \cdot 10^{-8}$	$7.5 \cdot 10^{-11}$
$4 \cdot 10^{11}$	$7.5 \cdot 10^{-9}$	$3.75 \cdot 10^{-11}$
$8 \cdot 10^{11}$	$3.75 \cdot 10^{-9}$	$1.875 \cdot 10^{-11}$
$1.6 \cdot 10^{12}$	$1.875 \cdot 10^{-9}$	$9.375 \cdot 10^{-12}$
$3.2 \cdot 10^{12}$	$9.375 \cdot 10^{-10}$	$4.688 \cdot 10^{-12}$
$6.4 \cdot 10^{12}$	$4.687 \cdot 10^{-10}$	$2.344 \cdot 10^{-12}$
$1.28 \cdot 10^{13}$	$2.344 \cdot 10^{-10}$	$1.172 \cdot 10^{-12}$
$2.56 \cdot 10^{13}$	$1.172 \cdot 10^{-10}$	$5.589 \cdot 10^{-13}$
$5.12 \cdot 10^{13}$	$5.589 \cdot 10^{-11}$	$2.93 \cdot 10^{-13}$
$1.024 \cdot 10^{14}$	$2.93 \cdot 10^{-11}$	$1.465 \cdot 10^{-13}$

In the presence of a hydrogen sublattice, the stoichiometric composition does not introduce phonon scattering points and the attenuation is not strongly different from pure palladium. It is different from the point of electron-phonon scattering since the electronic structure is different for PdH with respect to Pd. Another case for low phonon attenuation is a small hydrogen concentration in a metal lattice, corresponding to no more than a few percent atomic concentration. In other cases, phonons encounter an incomplete sublattice as an array of defects with high attenuation, thereby limiting the resonator length and amplification.

The following is an estimation of the phonon power density, which can be supplied by a resonator in this invention. The illustration has a piece of palladium foil excited by a thermal gradient of 1K along a 1cm length, with a foil thickness of approximately 10^{-4}m. The corresponding heat flow density is about $10^{4}W/m^{2}$. According to the Viedeman-Frantz law, the ratio of electron to phonon thermal conductivity components in a metal is about 3:1, or the heat flow attributed to phonons is about $3 \cdot 10^{-3}$W. If a resonator intercepts 1% of this heat flow, $3 \cdot 10^{-5}$W remain.

In a crystal, the phonon energy flux concentrates along certain directions and de-concentrates along others. This anisotrophy is called phonon focusing (*See* Narayanamurti, V., *SCIENCE* Vol. 214, No. 4509 (14 August 1981), pp. 717-723, the contents of which are incorporated herein). Theoretically, according to Taborek et al., the phonon intensity becomes extremely large in some instances, which is similar to optical resonators (*See* P. Taborek and D. Goodstein: Solid State Communications, No. 33, 1191 (1980)). Directional bottlenecks are called caustics and the same limitations apply. In an optical resonator, the caustic's width cannot be less than a couple of wavelengths (diffractional limit). Hence, for a phonon frequency of 10^{13}Hz ($\lambda \approx 2$Å) (refer to Table 2), the diffractional focusing area limitation is about 4Å^2. Since the focusing depends on the wavelength as λ^{-2}, a higher power density is obtained at higher phonon frequencies. Using directional phonon focusing at a phonon frequency of 10^{13} Hz, an upper theoretical power density limit of $3 \cdot 10^{-7}$w/$4 \cdot 10^{-20}$m$^2 \approx 10^{12}$W/m^2 can be obtained. Realistically, power densities of 10^7 - 10^8 W/m^2 are achievable by this method.

The phonon flux through the metal foil can be defined from thermal conductivity considerations. It is well known that the thermal conductivity of a metal, λ, is defined by electron and phonon components $\lambda = \lambda_{ph} + \lambda_{el}$. For most metals, the relationship between these components looks like $\lambda_{ph} \approx 1/3\ \lambda_{el}$. The thermal flux q through the foil with a temperature T_1 on one side and T_2 on the other side ($T_2 > T_1$) can be written as:

$$q = \lambda \frac{T_2 - T_1}{\Delta \ell} \cdot S,$$

where $\Delta\ell$ is the foil length, and S is the cross section area. The corresponding phonon flux q_{ph} equals $0.25q$. For example, a palladium foil with a thickness of 100 microns and 1 x 1 cm^2 area at a temperature differential of 10K (T_2 - T_1 =10K) will have a phonon flux of $1.55 \cdot 10^{-2}$ W, or a phonon flux density along the foil of $1.55 \cdot 10^4$ W/m^2, or about 10^4 eV/s per lattice site.

The minimal phonon flux required to achieve a sustained resonance can be addressed from attenuation/amplification considerations. The phonon intensity

change due to attenuation of a phonon mode with a frequency ω_o, follows the equation: $I_1 = I_o \cdot e^{-\alpha x}$, (see equation (3)) where I_o is the initial intensity, α is the attenuation, and x is the distance. At resonator length L, x equals L.

In a one dimensional model which considers the resonating media with the width much larger than the length, the number of lattice sites M equals L/d, where d is the lattice parameter. For a face centered cubic metal lattice (F.C.C.), i.e., palladium, an atom at each site has 3 directions with exactly the same properties; possible polarization can add a factor of 2. Hence, the directional factor in the amplification is 6, or the amplified part of a mode will be $I_o/6$. With a reflection coefficient on a resonator face r at normal incidence, the amplification follows the equation:

$$I_2 = \frac{I_o}{6} \cdot \frac{L}{d} \cdot r \qquad (4)$$

The mode will resonate when the amplification exceeds the attenuation, or when:

$$\frac{\partial}{\partial x}(I_1 I_2) > 0 \qquad (5)$$

or, $$\frac{\partial}{\partial x}\left(\frac{I_0 r x}{6d} e^{-\alpha x}\right) > 0$$

Differentiating this expression by length x, a maximum is found at $x = 1/\alpha$, which resembles the results for optical resonators.

Equation (5) allows for an estimation of the optimal L_{opt} and maximum L_{max} resonator thickness for Ni single crystal with <110> orientation, which are shown in Table 3, for a reflection coefficient r = 50% at 300K.

TABLE 3

Phonon Frequency ω, Hz	L_{opt}, Å	L_{max}, Å
10^{11}	$1.0 \cdot 10^{6}$	$9.7 \cdot 10^{6}$
10^{12}	$1.0 \cdot 10^{5}$	$7.5 \cdot 10^{5}$
10^{13}	$1.0 \cdot 10^{4}$	$5.4 \cdot 10^{4}$
10^{14}	$1.0 \cdot 10^{3}$	$3.1 \cdot 10^{3}$

For nickel polycrystal at 300 K the values are shown in Table 4:

TABLE 4

Phonon Frequency W, Hz	L_{opt}, Å	L_{max}, Å
10^{11}	$0.6 \cdot 10^{4}$	$4.8 \cdot 10^{4}$
10^{12}	$0.6 \cdot 10^{3}$	$2.5 \cdot 10^{3}$
10^{13}	60	60
10^{14}	6	6

In most cases, it is beneficial to keep the resonator length as long as possible because the higher the volume, the stronger the net effect is. The physical limitation from equation (5) is a layer thickness of 35 - 50Å, depending on the lattice parameter *d*. For palladium (d≈ 4 Å), layers thinner than 48Å will not work.

The example amplification obtained from equation (5) for the strongest phonon mode in a Pd-H system (1.3×10^{13} Hz), is shown in Figure 2, which is an example of a resonator mode behavior.

In some aspects, a phonon resonator is similar to an optical resonator, which means that some of the laser principles can be applied. First, similar to lasers, there is an excitation threshold, depending on the attenuation and resonator quality. A stable or unstable resonator is preferable, depending on the excitation level. The present invention deals with low phonon excitation levels, therefore, stable resonators are

preferred. Since the phonon wavelength is comparable to the lattice constant, resonance is always localized in space because of reflecting layer irregularity. A superlattice-type structure does not have these limitations. Moreover, resonator thermal stability issues have similar complexity to stable gas laser resonators.

The present invention deals with a 10^4 times shorter wave-length and a 10^4 times shorter resonator length than a typical gas laser. For palladium having a thermal expansion coefficient of about $1.1 \times 10^{-5}K^{-1}$, and at a distance between reflecting layers of 1 micron, the allowed temperature change, according to Table 2, is less than 0.05 K for $\omega = 10^{13}$ Hz during the experiment. A lower resonator length provides a more relaxed situation in terms of thermal stability. Since a 0.05K stability is close to a practical limit in most of the experiments, 1 micron long resonators may be the practical length limit imposed by thermal stability.

As an alternative, if thermal stability cannot be provided, thermal cycling over the thermal expansion exceeding $\lambda/2$ will provide for about 4 % of the time in resonance. In the example of 1 micron thick palladium at a resonance frequency of 10^{13} Hz, the resonator must be cycled with about a 10K temperature difference. This approach is reasonable if a resonator is built on the basis of a random grain size distribution, where the grain surface functions as a phonon reflector. In a general case for a material with a grain size L, thermal expansion coefficient K, resonant phonon frequency ω_o and speed of sound c, the thermal cycling amplitude ΔT will follow the equation:

$$\Delta T = \frac{c}{2\omega_o KL}$$

For a planar Fabri-Perot resonator with length L and quality Q, the temperature must be stable in order to maintain a resonance according to the relation:

$$\Delta T_2 \leq \frac{c}{2\omega_o QLK} \qquad (6),$$

where c is the speed of sound, ω_o is the resonant phonon frequency, and K is the thermal expansion coefficient. The condition of equation (6) is very undesirable and brings down the ideal Fabri-Perot type resonator performance to 4% of the time in the previous example with thermal cycling, thereby diminishing its utility. One way to

use a Fabri-Perot resonator is to apply a thermal gradient along it, which assures that the thermal expansion along the resonating layer will overlap half of the resonant phonon wavelength. Another method is to use a low amplification thin layer and tune it exactly using the temperature as a parameter. However, such a device is very complex for this embodiment.

According to the example in Table 3, the resonance width at a phonon frequency of 10^{13} Hz is probably $\frac{\Delta\lambda}{\lambda} \approx 2\%$. If the resonator length consists of m atomic layers (m - integer), a resonant condition is as follows:

$$md = \frac{n\lambda}{2} \pm 2\%, \qquad (7)$$

where both m and n are integers, and d is a lattice parameter. The lattice parameter for PdH varies from 4.0 to 4.1Å, with the hydrogen concentration varying from $PdH_{0.6}$ to $Pd\ H_{1.0}$. A three-dimensional patched graph illustrating resonant conditions is shown in Figure 3, where the x-axis is md, the y-axis is $(n\lambda)/2$, and the z-axis is the ratio x/y. The valley patterns on Figure 3 repeat themselves after about 30-40 steps, where a minimal span of L guarantees a resonance with crystalline structure of approximately 120-160Å. To ensure a broad band phonon resonance (from phonon frequencies of $2 \cdot 10^{11}$ Hz), the span of L must be more than 2250Å. Using vacuum deposition techniques or other comparable techniques known by those skilled in the art, it is possible to form a wedge-like structure 1 (see Figure 4), where the purpose of wedge-shape is to ensure a phonon resonance at a particular span along the wedge. The idealized distribution of atomic layers in this structure is shown in Figure 4 (dimensions set forth in Example 3 hereafter). In this structure the conditions of equation (7) can be fulfilled at any given temperature and resonant frequency, as long as the span in m numbers is large enough, i.e., more than 100. This approach provides for a broad-band multi-layer structure, which covers all possible phonon frequencies. Attenuation is a limiting factor and does not allow a broad-band resonator to be designed with only one layer, since the lower frequencies require thicker layers for which attenuation at higher frequencies is too strong.

A broad band stable phonon resonator 2 is shown in Figure 5. This structure utilizes the advantages of a wedge layer and focusing, thereby providing for various resonator lengths L along the structure. It is considered a stable resonance in the sense that a separate mode does not leave a certain region. This structure can be provided by different technological approaches discussed hereafter.

Non-Planar Geometries

A variety of non-planar resonator geometries are possible. According to Tables 2 and 3, for most of the frequencies a reasonable attenuation with sufficient amplification can be achieved in 3D structures less than 1 micron long, if the reflecting surface is sufficiently smooth, since non-uniformities function as scattering centers. For example, small crystallites having cubic structures of 10^{-6} m size may be utilized. Thin wires will provide a stable resonator in at least two dimensions with a preferred wire diameter of less than 10^{-6} m (see Fig. 8). A macroscopic resonator based on this approach must have an oriented structure, since, in the case of a coil for example, a phonon flux excited on one side will tend to compensate itself on the other side. A stack of microwire resonators 3 excited by a thermal gradient is shown in Figure 6.

The ultimate embodiment for a resonator is a three-dimensional stable resonance structure, which is either spherical, elliptical, segments thereof, or combinations thereof. These structures will resonate with all phonon frequencies, wherein the sphere has one focal point 4 and the ellipse has two focal points 5. A phonon standing wave structure for a sphere and ellipse is shown in Figures 7 and 8. Spheres having a diameter less than one micron can be obtained, such as by plasma-spraying, ball mill methods or other methods well known by those skilled in the art.

Etching small spheres in a high molarity electrolyte can remove surface irregularities smaller than 20-50Å. Amorphous spheres have a much smoother surface, since crystalline edges are absent. Such small particles cannot be free-standing and require a supportive envelope. A macroscopic spherical resonator with phonon excitation provided by a thermal gradient is shown in Figure 9. Particles 6 made of a two-component lattice, i.e., PdH(D) are enclosed in a supporting

envelope 7, which must have a low thermal conductivity in order to not waste the thermal gradient from temperatures T_2 to T_1.

Reflecting Layers

Reflecting layers for a stable and unstable two-component lattice are discussed separately. Also, reflecting layers are not required for 3-dimensional resonators or thin foils, since the phase boundary, i.e., metal-gas, functions as a reflector.

The example of an unstable 2D resonator is a planar PdH(D) structure. Because of the high diffusivity of hydrogen in palladium, a reflecting material (heavier than palladium) must be transparent to hydrogen diffusion. Elements such as Au, Pt, W, Ir, are not preferred as reflecting layers. Preferred materials are Ta, Hf, Re, Os, which have elastic constants very different from Pd that assure good reflection. When the exact resonance frequency is known, numerous efficient interferention layers can be designed, such as materials with different elastic constants that have different phonon spectra. A stack of thin foils will also work. Otherwise, the reflecting layers must be sufficiently massive, i.e., more than a few atomic layers, to ensure reflection. It also must be a few phonon wavelengths. Hence, for a 10^{13} Hz frequency, the reflecting layer thickness should be more than 20Å, and for a 10^{11} Hz the thickness should be more than 200Å.

For stable hydrides such as ZrH operating at temperatures below 100-200°C where the hydrogen loss is relatively small, most of the heavy elements can be used as reflecting layers. For refractory compositions such as carbides, reflecting layers may be deposited on the thin resonator layers. Using intercalated structures, in principle, provides for the use of intercalated layers of atoms, i.e., in graphite, for both phonon reflection and resonance at atomic levels with phonons.

Phonon Resonator Excitation

Numerous methods for exciting a phonon system in a solid-state exist. Most of these methods were developed to create a transient phonon flux. The best known method is a thermal pulse method, wherein a phonon flux is created by a thermal wave. The thermal wave can be initiated by a wire explosion, an arc spot or a laser

pulse. In the present invention, a sustained phonon flux is required, and transient methods do not suffice. The most evident way to achieve a sustained phonon flux is to create a permanent thermal gradient. Methods for creating a thermal gradient include placing a heater on one side of the resonator and a heat sink on the other, or placing heat conducting contacts on one or more sides of the resonator, or placing a convective heat exchanger device on one or more sides of the resonator. It should be noted that convective heat exchange may result from immersing the resonator in a liquid or gas without requiring a device. Other methods for creating a permanent thermal gradient include application of an electron flux, an acoustic flux, a diffusion flux, an AC magnetic flux, an electron beam, an ion beam, a plasma beam, gas dynamic flow, liquid flow, and radio frequency electromagnetic radiation. One skilled in the art will recognize there are numerous devices and methods for creating a permanent thermal gradient. The gradient orientation is preferably along the resonator from a technical standpoint, though any other orientation operates in the same way as the distance between reflecting layers (one micron or less) is much smaller than the physical size of a resonator. Acoustic radiation is less efficient, since a low frequency acoustic oscillation can be converted into phonon frequencies through thermal effects only. Thermal cycling effects were discussed previously. Direct phonon excitation methods can also be utilized, preferably normal to the resonator surface rather than on the side. These methods include application of a photon flux (infrared radiation, optical flux) and microwave radiation, which operate through electron-phonon interaction in a skin layer.

Threshold Effect from Anderson Localization Theorem

As discussed previously, to comply with Anderson's condition, the energy replenishment to the phonon mode at one lattice site must be more than the energy transfer from this mode to the nucleus. Replenishment goes through dipole-dipole interaction of neighboring phonons, which is about 10^{-4} eV/cycle of a phonon frequency of 10^{13} Hz (*See* Landau et al., *The Classical Theory of Fields*, pp. 97-101). This value is at least 4 orders of magnitude higher than the values for phonon dipole interaction with the quadrupole moment of the nucleus. Hence, as long as the phonon

density is sufficient, there are no energy replenishment limitations. However, the phonon density itself can present a problem. The phonon spectral density for a phonon flux q is a function of the phonon spectral distribution and the resonator line width, or the density equals $I(\omega)\Delta\omega$. In practical terms, it is more convenient to use the phonon wavelength and not the frequency, since the resonator line width $\Delta\lambda = \lambda^2/2L$, where λ is the wavelength and L is the resonator length.

Using normalization $\int_o^\infty I(\omega)d\omega = \int_o^\infty I(\lambda)d\lambda = 1$, and Figure 1 as $I(\omega)$, the result is $I(\lambda)$ as shown in Figure 10. For a phonon flux excitation with a thermal gradient ∇T for a material with a thermal conductivity κ, the spectral phonon density is as follows: $0.3I(\lambda)\Delta\lambda \cdot \kappa\nabla T \cdot F \cdot e^{-\alpha L}$, where 0.3 is the sequence of the Viedeman-Frantz law (ratio of the phonon thermal conductivity component to the total thermal conductivity), $I(\lambda)$ is the spectral phonon distribution, $\Delta\lambda$ is the resonator line width, F is the phonon focusing factor, and $e^{-\alpha L}$ is the attenuation at the resonator length. To obtain a flux through one crystallographic site, equation (8) must be multiplied by d^2, where d is the lattice parameter. To comply with Anderson's theorem, the final equation is as follows:

$$\frac{0.3F \cdot I(\lambda)\lambda^2 \cdot \kappa\nabla T \cdot e^{-\alpha L} \cdot d^2}{2L} > \frac{D\omega}{6\pi} \frac{\partial^2\varphi_o}{\partial\alpha\partial\beta} \quad (8)$$

The right side of the equation can be substituted for the case shown in Figure 11, assuming that a light sublattice element creates a dipole with amplitude $d \cdot \frac{\hbar\omega}{E_v}$, where $\hbar$ is the plank constant, E_v is the energy of the vacancy formation (triangle potential well). The dipole size dependence on the phonon frequency is illustrated in Figure 11. Substituting the dipole size and effective charge of a light atom e^* ($e^* = 0.6e_o$ for PdH), the following equation is obtained:

$$\frac{D\omega}{6\pi} \frac{\partial^2\varphi_o}{\partial\alpha\partial\beta} \approx \frac{De^*\omega d\frac{\hbar\omega}{E_v}}{2\pi x^4 o} \quad (9),$$

where D is the quadrupole moment of the nucleus, ω is the phonon frequency, E_v is the light atom, (i.e., hydrogen) vacancy formation energy (E_v for hydrogen in a near-stoichiometric lattice is about 0.5 eV; hydrogen trapped on a dislocation or host lattice vacancy 0.2 - 1.0 eV and up to 2.5 eV for carbides, nitrides, etc.), and x_o is the distance from the vacancy to the nucleus.

For $PdH_{0.67}$, $\nabla T = 1K$ and $\omega = 10^{13}$ Hz, the left side in equation (8) results in only 5 eV/s without focusing. For most resonators $F = 10^2 - 10^4$ (F is the ratio of energy density on the reflective surface and at $\lambda/4$). If $F= 10^3$, the threshold condition will be achieved at $\nabla T = 2K$.

Using equation (9), equation (8) can be rewritten as:

$$\frac{0.3F \cdot I(\lambda)\lambda^3 \cdot \kappa\nabla T \cdot d \cdot e^{-\alpha L}}{LC} > \frac{De^* \frac{\hbar\omega}{E_v}}{\pi x^4 o}, \quad (10)$$

where F is the focusing parameter, $I(\lambda)$ is the spectral phonon distribution, λ is the phonon wavelength, κ is the thermal conductivity, d is the lattice parameter, α is the phonon attenuation coefficient, L is the resonator length, c is the speed of sound in the lattice, D is the quadrupole moment of the nucleus, e^* is the vacancy effective charge, $\hbar\omega$ is the phonon energy, E_v is the energy of vacancy formation, and x_o is the distance between a nucleus and a vacancy.

The phonon spectral density is dependant upon the temperature. The temperature gradient is a more efficient way to increase the spectral density. For example, the calculated gain for absolute temperature 15 and the thermal gradient 17 for palladium with an initial temperature of 300K is shown in Figure 12.

Grain Size in a Polycrystal

Unless a metal is specially treated, the grains are distributed with random size and boundary orientation. The size distribution can be approximated by a Gauss or normal distribution, normalized on the mean grain size. The probability of obtaining a grain with a given size is described by the following formula:

$$P(x) = \frac{1}{\sigma\sqrt{2\pi}} e^{-\frac{(x-a)^2}{2\sigma^2}},$$

where a is a mean value and σ is a mean square deviation, and a corresponds to 10 microns and σ is assumed to be 3 microns. This is a very common situation with most metals. The number of grains with 1 micron size (optimum) will be 10^{-3}. With the sample size 0.1 cm^3, it corresponds to 10^8 of such grains. With a 1 micron long grain boundary on one side and a completely random situation with each adjacent atomic layer having to choose from 4 crystallographic directions in one dimension and 16 in two dimensions (for FCC lattice), the probability of getting a first order reflection is $(1/16)^n$. With n = 10, the probability of having a single resonator in this sample is approximately 10^{-4}. In reality, most of the samples are being subjected to mechanical treatment, such as rolling, which results in a crystallographic texture. With the same assumptions as before, a 50% texture results in a 10^3 times increase in the probability of obtaining a resonator, or about 10%. The situation is different for low phonon frequency resonance which can use larger grains. Since the energy transfer depends on the phonon frequency as ω^{-2} and assuming a reaction time of 10^2-10^3 s for $\omega=10^{13}$ Hz, a 10^{12} Hz reaction time will be 10^4 - 10^6 s, and 10^6-10^9 s for 10^{11} Hz, which is not acceptable for most practical applications.

These simplified examples demonstrate a method to build a resonator on the basis of a polycrystal, where (1) the grain size must be as small as possible, and (2) the sample must be textured, i.e., cold rolled with minimum annealing. Also, residual deformation can create wedge-shaped reflecting structures.

The probability of obtaining the effect improves with the excitation level. Estimations (not given here) show that structures having a thickness of a few millimeters can produce a stable phonon resonance at a phonon flux between 10^6-10^7 W/m^2. This is due to attenuation reduction in resonator caustics and the fact that the phonon density is very high. From a practical point of view the resonance width at such large distances is extremely narrow, with all of its associated technical difficulties. Thus, it is practical to keep the resonator length below at least 100 microns, even though the theoretical limit for a diamond lattice is about 10cm.

Other preferred lattices may comprise a polycrystal material with average grain size of about 10^{-6}m at a phonon flux of about 10^4 W/m^2, 10^{-5}m at 10^5 W/m^2, or 10^{-4}m at 10^6 W/m^2, or a single crystal material with the distance between phonon reflecting surfaces less than about three times the average grain size given before.

Monocrystal

The first component of the lattice may comprise a single crystal material having crystallographic orientation <110> between phonon reflecting surfaces for materials with face-centered-cubic structures.

Alternatively, the first component may comprise a single crystal material having crystallographic orientation <100> between phonon reflecting surfaces for materials with body-centered-cubic structures.

The first component may also comprise a single crystal material having crystallographic orientation <1000> (c-axis) between phonon reflecting surfaces for materials with hexagonal closely packed lattices.

As can be seen from Tables 3 and 4, single crystal materials are preferred over polycrystalline materials. A limitation of single crystals is that their manufacturing technology involves high temperatures that anneal vacancies and dislocations within the structure. Single crystals without vacancies are great conductors of hydrogen. However, stable hydrogen vacancies, which are required in the present method, are infrequently found in single crystals. To avoid this problem, a single crystal must be "aged" by known quenching techniques, or vacancies must be introduced by methods such as ion bombardment. Thermal cycling increases the number of vacancies by up to 18% (See Fukai et al. "Formation of Superabundant Vacancies in Pd Hydride under High Hydrogen Pressures." *Physical Review Letters*, vol. 73, no. 12 (Sept. 19, 1994), pp. 1640-1643, the contents of which are specifically incorporated herein.) In the case of ion bombardment, heavy ions are preferred since they give more vacancies per ion (evaluations can be made by TRIM-91™ Software, IBM, 1991). Non-hydride lattice combinations such as carbides have more stable vacancies and do not require any treatment. Creating a dislocation field for hydrogen trapping is beneficial in all

hydride lattices and can be achieved by creating a residual deformation in the material.

Vacancies are dynamic objects in a solid-state lattice, which move from one place to another. Since static vacancies are required, only vacancies having a sufficient life-time of a few seconds are of concern. The probability of moving a vacancy from its original place, w, is as follows: $w = w_0 e^{-\frac{E_a}{\kappa T}}$ where E_a is the vacancy activation energy, κ is Boltzman's constant, and T is the temperature. The primary process is the activation by high frequency phonons, i.e., $E_a = \hbar w$, where $\hbar$ is Plank's constant and w is the phonon frequency. The energy transfer goes through the phonon momentum transfer $E_a = \frac{P^2}{2m} = \frac{(|\hbar\kappa|)^2}{2m}$, where κ is the phonon wave vector and m is the mass of the vacancy involved (vacancy is understood in both a positive and negative sense). If there is a choice between hydrogen ($m = 1$) and deuterium ($m = 2$), the required phonon momentum for deuterium (P_2) will relate to the phonon momentum for hydrogen (P_1) as $P_2 = P_1\sqrt{2}$. Assuming a Boltzman distribution of phonon energy and substituting (2) into (1), the resulting ratio is $w_2/w_1 = e^{-2} = 0.135$. The deuterium vacancy is approximately 7.4 times more stable than the hydrogen vacancy, resulting in a 7.4 times stronger effect.

Only static hydrogen (or other light component) vacancies associated with dislocations, impurities and host metal vacancies have been assumed to take part in energy transfer. Due to a very large number of light component atoms, even jumping vacancies form a group, which is statistically static long enough to be treated as static vacancies for the present invention. According to Alefeld, G. "Hydrogen Diffusion in Metals." in: *Vacancies and Interstitials in Metals*, (North-Holland Publishing Company, Amsterdam, 1970, Proceedings of the International Conference held at Jülich, Germany, 23-28 September, 1968, pp. 959-971), jumping frequencies for oxygen or nitrogen interstitials in metals are about 10^2 jumps/ sec. If a sample contains 10^{22} light element atoms and the required time for energy transfer is 10^2 seconds, then 10^{18} sites can be regarded as static vacancies. The hydrogen situation is

different because its diffusivity is many orders of magnitude higher than that of oxygen or nitrogen.

Following Alefeld, the mean jump probability for deuterium in palladium can be written as: $\tau^{-1}(C_D) = (1 - C_D) \times 10^{13} \cdot exp(-0.19\ eV/\kappa T) + (10^{10}) \cdot exp(-0.13\ eV/\kappa T)$, where C_D is the deuterium concentration, κ is Boltzman's constant, and T is the temperature. The second additive give the jump probability, when D/Pd ≡ 1, which corresponds to $5 \cdot 10^7$ jumps/s. This case corresponds to the absence of vacancies and is not pertinent to the present invention. For all practical purposes, the second additive is smaller than the first and can be neglected.

Considering a palladium sample having 10^{22} atoms (1.5 grams) at room temperature and a $10 - 10^2$ s energy transfer time to the nucleus, a D/Pd = 0.99 concentration provides $5 \cdot 10^{11} - 5 \cdot 10^{12}$ "statistically static" vacancies. A D/Pd = 0.99 concentration provides $5 \cdot 10^{12} - 5 \cdot 10^{13}$ of "statistically static" vacancies.

EXAMPLE 1

A cross-section of the experimental chamber 10 is shown in Figure 13. All major parts of the device are made of 316 stainless steel. The internal diameter of the active tube 12 filled with palladium powder 14 is 0.228" (5.8 mm), and the powder 14 filled length is 1.78" (45mm). The outside diameter of the tube 12 is 0.575" (15 mm). The powder is contained by a porous stainless steel filter 16 (KRESOGE SF - 20) on both ends of the tube 12. The filter 16 itself is compressed by threaded nuts on both ends. The upper part 22 of the active tube 12 is welded with a massive 8" diameter upper flange 24 with a 1" thickness. This upper flange 24 has vacuum feed-throughs 26 for up to 6 thermocouples 28 and two electric leads. At the bottom end of active tube 12 and adjacent to filter 16 is a stainless steel bushing 19, which is sealed off at its lower end with plug 21.

Figure 14 shows a perspective view of the experimental chamber 10 with the flange 24 having feedthroughs 26 for 5 thermocouples 28, 2 electrical leads for the heater 32, and a thermocouple 28 for the heater 32. The lower flange 34 with a cup shaped main chamber 36 is sealed by Viton™ gaskets 38. The main chamber 36 has a connection for a vacuum system and forms a vacuum thermal insulation around the

active tube 12. The heater 32 is made of AMPTEK quartz fiber insulated with alumel wire, which is rated to 1100°C. The radiation screen 40 around the heater 32 is made either from the same wire or 4 mil thick SS 316 foil.

Four OMEGA T-type thermocouples 28 are clamped to the active tube 12, allowing two independent readings of the thermal gradient. An additional OMEGA K-type thermocouple 29 is used to monitor the heater 32 temperature.

The heat flow along the tube 12 (assuming thermal conductivity of the powder 14 itself to be negligibly small) can be written as: $q = \lambda \frac{\nabla T}{\nabla X} S$, where λ is the thermal conductivity of the stainless steel, S is the tube 12 cross section (1.36 cm^2), and ∇X is the measured length between the thermocouples (3.2 cm). The tube 12 diameters were machined to better than 0.1 percent tolerances. The thermocouple size (1 mm) introduced a 3% error in ∇X measurements. The layout for the experiment is standard for thermal conductivity measurements. This allows the thermal conductivity of stainless steel to be determined for the experiments. This step is important because the data from reference books varies significantly for different batches of stainless steel of the same brand.

At low temperatures and low thermal gradients in a high vacuum, the only pass for heat flow from the heater is through the stainless steel tube. Radiation losses at temperatures below 100°C are negligibly small, since they follow Stefan-Boltzmann's law of $q = \sigma T^4$. Experimentally determined values for the thermal conductivity were λ = 28.8 +/- 1.7 W/(m·K). This provides a coefficient to calculate the heat flow at room temperature, $\kappa = \lambda(S/\nabla X) = 0.122$ W/κ. The absolute error is 6.5%, and the relative error is around 3.5% near room temperature. The error is 1% when the temperature is greater than 300°C. The change in stainless steel's thermal conductivity with temperature was treated as a loss and was automatically included in the calibration curve.

1. VACUUM SYSTEM

The schematic for the vacuum system 42 is shown in Figure 15. The dry vacuum system 42 is built around a Pfeiffer Vacuum TMU 065 turbo molecular pump 44, which provides 10^{-9} torr vacuum. A GAST ROC-R diaphragm pump 46 was used for a rough vacuum in series with the turbo molecular pump 44. Both the turbo molecular pump 44 and the diaphragm pump 46 were air cooled by outside fans. A major vacuum lock was provided by a MDC AV - 250 UHV valve 48. A Balzers Compact Full Range gage 49 provided for 100 - 10^{-9} torr measurements with readings from a Balzers single gauge display 50. All flanges were Conflat™ with copper gaskets. The connections to the UHV gas line 51 were Cajon VCR™ with nickel gaskets, and the connections in the HV gas line 52 were Swagelock™. Nupro 55-6 BW valves 54 and a Nupro SS-4H-TH3 56 valve were used throughout the system. Bypass line 58 serves as a bypass to the UHV gas line 51. A flexible stainless steel hose 62 was utilized in providing a vacuum in tube 12. Care should be taken to avoid oil from the pump 44 making contact with the powder 14.

The standard pressure in the UHV line 51 was 1 - 2 x 10^{-7} torr, with the best values around 5 x 10^{-8} torr after a few days of pumping and baking. The standard achievable pressure in the HV line 52 was around 10^{-6} torr.

2. GAS SYSTEM

The gas system 63 is shown in Figure 16 and consists of two subsystems, a "dirty" (HV rated) and a "clean" (UHV rated). All lines are comprised of stainless steel tubes, except the release tubes, which are 1.5 mm ID copper tubes. The "dirty line" connectors are Swagelock™ standard and all of the "clean line" connectors are Cajon VCR with nickel gaskets, rated to 10^{-11} cc/torr x sec. leak rate. The valves 56 in the "dirty lines" are Nupro SS-4H-TH3 bellows valves rated to 10^{-9} torr closed, and the valves in the "clean lines" are Nupro SS-6BW bellows valves 54, rated to 10^{-9} torr in any position.

The centerpiece of the system is the Resource System, Inc. hydrogen purifier 68. The purification process is based on gas diffusion through a palladium filter at high temperature. Gas to the purifier 68 is supplied through the "dirty"

line 70, and the purified gas goes to the "clean" line 72. From the high pressure cylinder 74, active gas (D_2) goes through the Harris pressure regulator 76 to the gas purifier 68. Before the gas is introduced, the line 70 is pumped down. Because D_2 is a flammable gas, line 70 has an argon gas purge system 78 (including pressure regulator 79) and a gas release valve 56.

The clean line 72 can be pumped through the active tube 12 and through the UHV bypass 58. A separate bypass line 51 allows the working chamber to be refilled with high pressure gas without stopping the experiment. The "clean" line 72 also has a MKS Baratron^R type 750B capacitance pressure gauge 80 with a 35 atmosphere range and 0.5% precision. The gas pressure is displayed by a digital MKS PDR-C-2C readout/power supply. The maximum pressure in the line 72 is limited to 20 atmospheres (gas purifier limitation).

For safety purposes, a combustible gas monitor by Sierra Monitor Corp. model SMC 2001 was included in the installation.

3. POWDER PREPARATION

The powder mix 14 consisted of two components, Johnson Matthey palladium powder (0.25 - 0.55 microns, 99.95% pure) and Aldrich palladium powder (1.0 - 1.5 microns, 99.9+ % pure). Equal volumes of the components were mixed in a horizontal glass mixer with rubber seals at 60 RPM for two hours. Scanning electron microscope photographs of the powder samples showed that most of the particles had a near-spherical shape. The approximate powder 14 load in the system was three grams.

4. TEMPERATURE MEASUREMENTS

Four thermocouples 28 were used to measure the temperature gradient. The cold side thermocouples 28 were placed at various locations, as illustrated in Figure 13, to get an idea of the temperature profile along the tube. One pair of thermocouples 28 was connected to a programmable Keithly 2001 digital multi meter, providing 0.1 degree resolution and 0.5 degree accuracy in the entire temperature range.

The second pair of thermocouples 28 was connected to a Keithly Metrabyte DAS-8 data acquisition system through Keithly MB 30 isolated inputs, all of which were incorporated into the Micron Millennia Lxa P-166 computer. The data acquisition system provides for a 0.5 degrees resolution and a 1.7 degrees accuracy. The fifth thermocouple 29 (Omega K-type) was used for control purposes only, which measurements could be used with a Fluke 79 digital multi meter.

5. HEATER POWER SUPPLY

The power supply was based on a 2kW rated Variac. The Variac was connected to the mains via a safety device consisting of an Omega temperature controller for K-type thermocouples 29 and a 30 amperes rated, double insulated relay. A signal from the K-type thermocouple 29 placed on heater wire coils 32 was used for the controller input. The controller has about 2 degrees accuracy and was allowed to shut down the mains line when the heater 32 temperature exceeded a given value. The safety device allowed the system to be left unattended without a risk of overheating. The alumel heating wire (heater 32) was used in the experiments. Recording both the operating current and the voltage with Fluke 73 and 79 digital multimeters results in a 1% error bar in power readings.

6. CALORIMETER CALIBRATION

The system requires a separate calibration for each heater 32 configuration. This is evident, because radiation losses are different for each configuration, though conductive losses through the stainless steel tube 12 were the same. The change in the SS thermal conductivity was treated as losses and was included in the calibration curve. The calibration was held before each experiment in high vacuum conditions (without the gas). Gas, especially hydrogen at high pressure, has significant thermal conductivity, and the thermal losses in a vacuum are somewhat lower. Rough calculations give 2 - 3 watts of additional losses at 300°C for the design. These losses are not included in the present protocol, thus making the calibration conservative. Substituting the vacuum with 130 psi of argon gas does not change a calibration curve within the error bars.

The calibration consisted of heating the active tube 12 at a given power by means of the heater 32, waiting until the system reached thermal equilibrium, and measuring the output power as described previously. The time needed to reach thermal equilibrium depends on the final temperature (input power) and varies from 1 to 2.5 hours in the 50 - 350°C temperature range. Normally, a 3 - 5 hour time interval was utilized for calibration measurements. In the vacuum, or argon, after thermal equilibrium is attained, the temperature stays constant within 2 - 3 degrees for a given power and is highly reproducible, with a temperature variation of no more than 3 degrees from one run to another.

The calibration curve measured essentially the same for two heater wires of similar design, as shown in Figure 17. (The first heater wire inadvertently burned during the experiment after about 70 hours of operation.) The two sets of measurements were taken before the experiments and one after the experiments. Figure 17 shows that calibration is stable and does not exceed the cumulative relative error (approximately 3% at temperatures over 200°C).

7. EXPERIMENTAL PROTOCOL

The experimental procedure consists of the following steps:

1. loading the powder 14 and gently tapping it with a steel rod (Example 1 had a density of 18% for 2.6 grams of powder);
2. putting the filter 16 in place and compressing it;
3. wrapping the heater wire 32 and installing the radiation screen 40;
4. pumping down the "clean" vacuum line 72 to 10^{-7} torr range;
5. out gassing the heater 32 by heating it to 350°C;
6. baking the powder 14 in the UHV gas line 57 at an elevated temperature (300°C) for out gassing;
7. calorimeter calibration (can be combined with step 6);
8. pumping down the "dirty" gas line 70;
9. letting deuterium in through the gas purifier 68 (at 130 psi);
10. thermally cycling the powder 14 by gradually heating it to about 300-320°C at a rate of 10W increments every hour to 1.5 hour up to about

30W, keeping the temperature for 2-6 hours and then cooling it down for at least a 10 hour time interval to create stable charge vacancies in the metal hydride. (Note: cycling requires about 4 cycles; in the first two cycles the output lies well below the calibration curve in the entire temperature range; temperature excursions are noticeable from the third run); and

11. after the second to sixth cycle, the powder 14 preparation is completed and experimental runs may be considered live. Actual operating temperatures ranged from about 300°C to 420°C.

It should be noted that the requirement of maintaining orientational stability of the palladium nuclei is inherently accomplished through the spherical shape of the palladium powder and the earth's magnetic field.

8. EXPERIMENTAL RESULTS

The experimental curves plotted as power input and power output versus time are shown in Figures 18 and 19. The step curve represents the input power from the electric heater 32. The output curve exhibits the threshold effect. These figures relate to the experimental runs after several thermal cycles of the powder 14 with gas introduced. For a short period of time at a low heater power the system exhibits small amounts of enhanced heat generation. The output then drops and 50% of the power is sometimes lost. The maximum total loss in the energy balance was approximately 70 kJ. After 3 or 4 thermal cycles, the energy release increases and the experimental runs perform as shown in Figures 18 and 19, with the balance becoming positive. Thermal cycling is required with each gas change. Without thermal cycling, the output follows the calibration curve within experimental error. The plot of the cumulative energy balance is shown in Figure 20.

EXAMPLE 2

An all-wave phonon resonator was assembled utilizing a palladium media 108 and rhenium reflecting layers 109 (See Figure 21). Rhenium forms hydrides and, up to thicknesses of about 500 Å, is relatively transparent to hydrogen. To avoid thermal

expansion problems, the resonator structure was formed in a wedge shape with conditions continuously changing in the resonator thickness along its width, which was more than half of the corresponding phonon wavelength. This condition was extended to achieve at least 10-20 standing wave regions along the structure at any given phonon frequency. The thickness of the reflecting rhenium layers 109 were about a few phonon wavelengths to ensure at least partial phonon reflection.

Aldrich (99.98%) palladium foil having a thickness of 50 microns and an area of 50 x 50 mm^2 was used as a substrate 111. The resonating structure was deposited in a vacuum chamber. A two gun magneton sputtering device 113 (see Fig. 22) was utilized, with one gun for palladium and the other for rhenium.

Johnson Matthey Puratronic 99.9975% pure palladium was used for one sputtering target, and Johnson Matthey 99.97% pure rhenium for the other. A wedge-shape structure was achieved by displacing a substrate from the atomic beam center 115 and putting it at an angle to the beam axis 117, as shown in Figure 22. The layer thicknesses were measured during the calibration process with piezoelectric sensors having a glass plate repeating target geometry 119 as a substrate and with sensors placed closest to and farthest from the axis ends.

The configuration of the resulting structure is shown in Figure 21. The structure is a broad band phonon resonator with frequencies from at least about $5 \cdot 10^{10}$ Hz to $2 \cdot 10^{14}$ Hz. The deposition was conducted at a relatively low temperature, $T < 100°C$. During hydriding there are large stresses on the Re-Pd interfaces, which can lead to delamination. In order to avoid this problem annealing technology was utilized, by annealing small samples of the structure at 50°C increments in an infrared vacuum furnace and then analyzing the cross-sections. The thickest Re layer (200 Å) could be seen with a high resolution (50Å) scanning electron microscope (JEOL), since the contrast between Pd and Re is very good. When the Re layer lost its contrast, the interdiffusion level was considered unacceptable. As a result, the optimized annealing parameters were $550 \pm 50°C$ for 5 minutes. The annealed samples were repeatedly loaded in a heavy water electrolytic environment and exhibited satisfactory stability with respect to delamination after several hydrogen loading and deloading cycles for at least a few days.

The broad-band phonon resonator described above was tested in a glow discharge environment shown in Figure 23. The testing device was a water flow calorimeter 146 with separate water flow temperature measurements in three calorimeter parts, an outside envelope 148 which intercepts the radiative and convective heat flows and a cathode 150 and anode 152, which were disposed at the ends of heat flow components 154 and 156 having direct discharge current inputs. Each water input and output was supplied with temperature sensors and was measured together with the water flows by a data acquisition system (Keithley DAS-8). The accuracy of the calorimeter was about 0.1W in the 1-10W power input region and 0.3 - 0.5W for the 10-100 W power input region.

The water cooled envelope created a vacuum chamber 158 pumped down to 10^{-6} Torr residual pressure and filled with gaseous deuterium at a pressure of 2.6 Torr. During the fill-in, the gas was passed through high temperature Ti chips and a Pd foil filter, thereby providing for a gas purity in terms of O_2 and H_2O with quantities less than 0.1 ppm. The rectified electric power in (50Hz) was measured by integrating the current and voltage in each cycle: $P_{electric} = \int UId\tau$. The difference between the power measured by the calorimeter and $P_{electric}$ gave the power generated inside the device (if any). The calorimeter schematics are shown in Figure 23. The vacuum, gas, and measurement portions of the calorimeter are not shown. A phonon resonator foil (not annealed) was cut into discs 160 with 10mm diameters and installed in the cathode portions 162 and 164 of the calorimeters shown in Figure 24 and 25 respectively. The difference between Figures 24 and 25 is an additional thermal resistance in the form of a Cu disc 166 and Mo discs 168 (0.2 mm thickness) and 170 shown in Figure 25. The thermal gradient from the center of the sample to its periphery is probably 10-20 K/cm (50W) larger than it is without a disk (known from previous calibrations). The efficiency in terms of creating a thermal gradient was low ($\geq 10^{-4}$) in order not to destroy the resonator disc 160 (0.5 mm thickness) by overheating it. Specially annealed Pd foils were used as blanks to give a base line calorimeter calibration.

It should be noted that orientational stability of the palladium nuclei was maintained by means of the earth's magnetic field.

The test results are shown in Table 5, where sample A represents the results from the Figure 24 set up and sample B represents the results from the Figure 25 set up. Each run lasted approximately one hour. Table 5 shows the threshold character of enhanced heat production. The endothermic power regimes were probably energy storage. In terms of a signal/noise ratio, some of the runs show approximately 40σ results.

TABLE 6

SAMPLE (Picture)	ELECTRIC POWER in, W	POWER out, W	EFFICIENCY out/in
Blank 1 (A)	7.9	0	0.98
Blank 1 (A)	11.5	0	1.0
Resonator (A) (Beginning of Experiment)	6.3	negative*	0.90
Resonator (A) (End of Experiment)	4.5	0.2	1.05
Resonator (A)	18.3	4.5	1.24
Resonator (A)	8.2	4.9	1.6
Resonator (A)	24.2	5.1	1.2
Resonator (A)	35.7	8.5	1.24
Resonator (A)	43	11.6	1.27
Resonator (B)	7.6	0	1.0
Resonator (B)	15.4	0	1.0
Resonator (B)	29.7	6.3 - 8.4	1.21 - 1.29
Resonator (B)	61.9	21.5	1.34
Resonator (B)	44	10.5	1.22
*Energy Storage			

EXAMPLE 3

The preferred embodiment for a water heater application is shown in Figure 26. Stainless steel cylinders 110 with a 2.5cm diameter and 6mm holes along its surface are filled with samarium alloy microspheres 112 (having a diameter of 0.2 -

2 microns). The end of cylinder 110 is sealed with a palladium filter 114 (100 micron thick), which is welded in a vacuum to the cylinder 110 (welded joints are shown at 116). Cylinders 110 have screws 118, allowing thermal contact to the water cooled surface and quick changing of cylinders 110. Each cylinder 110 has a separate electric heater 120 (about 100w). Each cylinder 110 is capable of providing 250-300 W of thermal power. Therefore, four cylinders are needed to obtain a 1 kW water heater. A high pressure (up to 20 atmospheres) chamber made of stainless steel consists of parts 122 and 124, sealed with high temperature gasket 126 and bolts 140. Part 124 of the chamber is cooled by water which follows through the channel 128. The chamber has a gas inlet 130 with a high pressure valve 132 which can be connected to an external hydrogen or deuterium vessel (not shown) and then disconnected after filling. Part 124 has a high pressure electric lead 134, connected with a wire 142 to heaters 120. The device is insulated thermally from the environment with foamed insulation 136. The device has a permanent magnet 138 on the bottom for aligning the spin of the samarium nuclei to maintain orientational stability.

The device operates in the following manner: after pumping out volume 144, the gaseous hydrogen (or deuterium) fills a high pressure volume 144 through valve 132 and inlet 130 to a pressure of about 10 atm. The heaters are turned on and the hydrogen then starts to diffuse through the filter 114 to the microspheres 112. Hence, contamination on the microspheres 112 surface with oxygen, etc., is avoided. After about one hour, valve 132 can be closed and the device is ready for operation. After connecting the device to a water line, the heater 120 is turned on for about 20 minutes and then can be switched off. The thermal gradient caused by the heater creates a phonon resonance. Heat production can be stopped by applying a strong magnetic field normal to the cylinders 110 axis or by removing the hydrogen.

Alternative Theory

The inventor of the present inventions proffers the following alternative theory to a chemical reaction as the basis for the enhanced energy generation over the background art.

Phonons participate in most energy-transfer processes in solids. Phonons are lattice vibrations having a frequency in the range of 10^{11} - 10^{14} Hz. Lattice vibrations create an oscillating electric field, which can interact with the nucleus. The well-known example of phonon-nucleus interaction is the Mössbauer effect.

The recoil momentum of a gamma-quant emission of a radioactive element embedded in a solid state lattice can be coupled directly to the lattice phonon system (*See* Herber, "Mössbauer Effect" in *McGraw Hill Encyclopedia of Science and Technology* (1982), vol. 8, pp. 754-757.) The energy involved in this process is a fraction of an electron-volt, since the gamma-quant has a zero mass.

The ground nuclear level is split due to nucleon-nucleon interaction, the interaction of nucleons with electron shell, and so forth. *(See* Otten, E.W. "Introductory Remarks" in: Vergnes, M. et al. Ed., *Nuclear Shapes and Nuclear Structure of Low Excitation Energies*, NATO ASI Series, Series B: Physics Vol. 289, (New York, Plenum Press, 1992), pp. 3-13.)

According to D.I. Bolef and R.K. Sundfors, *Nuclear Acoustic Resonance*, Academic Press, 1993, the energy quantum levels resulting from the interaction of a nuclear quadrupole moment with a non-uniform electric field induced by an electric charge e in a crystalline lattice follows the equation:

$$E = \frac{e^2qQ}{4I(2I-1)} [3m^2-I(I+1)]$$

where q is the electric field gradient, Q is the nuclear quadrupole moment, I is the nuclear spin and m is the magnetic quantum number. In the absence of a magnetic field for rhenium 185 isotope (I=5/2), I + ½ double degenerate energy levels E_m exist with moment numbers $\pm$ 1/2; $\pm$ 3/2; $\pm$ 5/2, corresponding to two possible transitions at a frequency $V_Q = 3/20\ e^2qQ$ and $2V_Q$. In this instance, V_Q corresponds to $2 \cdot 10^{-8}$ eV.

The electric field gradient in a metallic crystalline lattice can reach high values in a two-component lattice, such as $2 \cdot 10^{22}$ V/m^2 for Te-W composition, due to antishielding effects. (*See* Bolef et al., *Nuclear Acoustic Resonance*, pp. 215-226)

Bolef et al. observed anomalies in a nuclear acoustic resonance (resonance between quantum levels induced by a magnetic field and other levels, resulting in absorption of magnetic field energy) line shapes in a Ta-H system (*See* Bolef et al., *Nuclear Acoustic Resonance*, pp. 188-191). They explained the effect on the basis of the interaction between the quadrupole moment of a ^{181}Ta nucleus with static charged defects in the crystalline lattice. However, they did not address the possibilities of amplification of the effect.

An analogy exists between a nucleus in a solid state lattice and an optical situation with Nd^{+++} glass lasers. Hence, a number of optics analogies can be applied to nucleus-phonon interactions. From solid state lasers, it is known that a combination of optical and acoustical energy transfer can result in up-conversion or emission of high energy photons resulting from low energy initiation. This effect requires the existence of intermediate atomic quantum levels with life-times longer than for higher energy levels, from which photon emissions can be observed. (*See* Auzel, F., "Multiphonon Processes, Cross-Relaxation and Up-Conversion in Ion-Activated Solids, Exemplified by Minilaser Materials" *in Radiationless Processes*, (New York, Plenum Press, 1979), pp. 253-256.) However, the radiative transition level's energy is the limiting factor, which if higher, allows the energy enhancement to also be higher.

Other optical analogies can be applied to the nucleus interaction with phonons, such as Anderson's localization theorem. (*See* Auzel, F., *Radiationless Processes* , pp. 250-251). Application of this theorem to the energy transfer from the phonon mode to the nucleus requires an intensive phonon mode, otherwise, energy transfer is prohibitive. An intensive phonon mode in resonance with the nuclear ground level will create up-conversion conditions, since the relaxation of these levels can only be achieved by cross-phonon relaxation or interaction with electrons. Cross-phonon relaxation can be made small artificially by creating thermal equilibrium conditions (discussed hereafter). Interactive relaxation through an electron system is random and

has a relatively low probability because of the limitations prescribed by the laws of conservation. The only possibilities are quadrupole-dipole and quadrupole-spin relaxation, discussed hereafter.

Following is a discussion of how phonons can interact with the nucleus. As stated above, lattice vibrations create an oscillating electric field, which can interact with the nucleus. Dipole interaction is absent because all nuclei do not have a dipole moment in their ground state. Some of the nuclei have a quadrupole moment, which can be viewed as a system composed of two dipoles of equal but oppositely directed moment. Quadrupole interaction gives an additional energy as follows:

$$E = e_o \frac{D}{6} \frac{\partial^2 \varphi_o}{\partial\alpha\partial\beta}, \qquad (1)$$

where D is the nuclear quadrupole moment, α and β are the coordinates, e_o is the elementary charge, and φ_o is the electric potential at the nucleus location in a crystalline lattice site (*See*, Landau, L.D. et al., *The Classical Theory of Fields*, Pergamon Press, 1975, pp. 97-101). At a phonon mode energy E of 0.01 - 0.1 eV ($E = \hbar\omega$, where $\hbar$ is Plank's constant and ω is the phonon frequency), a rough estimation gives an interaction energy accumulation of 10^{-8} - 10^{-11} eV per cycle, or 10^{-1} - 10^{5} eV per second in frequency ranges of 10^{11}-10^{14} Hz. To accumulate sufficient energy to alter a nucleus, a high frequency phonon mode must be sustained for at least about 100 seconds. In a two-component, solid-state lattice with vacancies, slow oscillations of a heavy nuclei system and fast movement of an electron system exist. The electric field changes due to nuclear system oscillations, which are effectively screened by electrons at a few lattice parameters. It is highly unlikely that neighboring sites will have strongly different sustained phonon modes, since they tend to attenuate each other. Anharmonic modes can exist at neighboring sites, but it is difficult to imagine sustainable anharmonic modes. The situation is different with a two-component lattice with different masses in each sublattice. In this case, harmonic oscillations of each sublattice are basically different, providing for a strong oscillating field at the nucleus location. The ideal case corresponds to near stoichiometric sublattices, or low concentrations of a second component. Phonons see sublattice vacancies as scattering

defects and the phonon mode attenuation increases, thereby making it difficult to achieve resonance conditions.

Following is a discussion of the two-component lattice shown in Figure 27. The combined lattice consists of a light nuclei with mass *m* and a heavy nuclei having a mass *M* and a spin S. Since the existence of a nuclear quadrupole moment of a nucleus is always associated with a nuclear spin $|S| \geq 1$, spin is always present. Assuming that a local magnetic field H vector exists along the x-axis and is sufficiently strong, it aligns spins S_i of nuclei M_i along the x-axis, and provides orientational stability. Nuclei that have a quadrupole moment correspond either to nuclei prolate along the spin orientation or oblate along S. As long as orientational stability exists, it does not effect the present invention.

If the lattice is in an equilibrium state, the nucleus M_1 (see Fig. 28) sits in a state with minimum potential φ_o , $\varphi_o = \min\varphi(x)^1$, and the total electric field is compensated, or $E_o = \frac{\partial \varphi}{\partial x} = 0$. The same is true for the electric field gradient, $\frac{\partial E_o}{\partial x} = \frac{\partial^2 \varphi}{\partial x^2} = 0$. The nucleus only sees the electric field gradient, due to the existence of the quadrupole moment.

In a complete cubic lattice due to its absolute symmetry, the net effect of the oscillating electric field on the nucleus will be zero with random deviations from stability, even for a higher multipole interaction. However, to achieve energy transfer, deviations from the stable state must not be random.

When $M >> m$ and the sublattice *M* is more stable than the sublattice *m*, the phonon oscillator strength is stronger for the sublattice *M*, for example, in the case of hydrides. This corresponds to the situation where oscillations of the sublattice *m* do not strongly change the position of the nuclei in the sublattice *M*. In other words, the phonon spectrum of the sublattice *m* is entirely different from that of the sublattice *M*. This case is illustrated in Figure 28, where the nucleus *M*, shown as a quadrupole, is sitting near the minimum potential point x_o, with its spin S aligned along the x-axis and looking at the x-component of the electric field created by movements of the sublattice *m*. As the spin S is aligned along the x-axis, the nucleus rotates about the x-

axis, with the nuclear rotation frequency typically in the 10^{20}Hz range. This frequency is much higher than the phonon frequency, and thus the nucleus sees any lattice movements along the *y* and *z* directions as being random.

If coherent oscillation of sublattice *m* along the x-axis are created, i.e., by amplifying a single phonon mode by a phonon resonator, the situation becomes much easier to understand. To break symmetry and to obtain energy transfer, mass m_4 is removed to create vacancy V_4. This situation now corresponds to an oriented quadrupole in a field of a single charge oscillating along the x-axis.

The oscillating charge position can be written as $x = x_o + \Delta\sin\omega t$, where x_o corresponds to the minimum potential and Δ is the maximum deviation from x_o. The characteristic size of the nucleus is about 10^{-15} - 10^{-14} m. The distance from the nucleus to the charge x_o is about 10^{-10} m, and Δ is about 10^{-11} m (amplitude of phonon oscillations). Making a reasonable assumption on the potential change of 0.1V along Δ, the electric field has a maximum of about 10^{10} V/m and $\frac{\partial^2\varphi}{\partial x^2}$ is about 10^{19}-10^{20} V/m^2. The effect on the nucleus is evidently asymmetric. The electric field is stronger in the case of a negative Δ and weaker with a positive Δ. On the length of the nucleus itself, the difference in the electric field strength is about 10^5 V/m. The nuclear deformation reaction time to the quadrupole electric field interaction is slow relative to the phonon frequency (about 10^3 times slower at the discussed energies, and each cycle adds energy). A simple estimation from the given geometry and elementary charges give a transfer rate of about 10^{-10} eV/cycle. More precise integration over the cycle with Q = 3 barn (for ^{181}Ta isotope) and one oscillating elementary charge, increases this value to about 10^{-9} eV/cycle at a phonon frequency 10^{12} Hz.

This can be illustrated by the following considerations. An electric field induced by a phonon oscillation can be significant only within a lattice site, or within about 1Å distance from a vacancy, elsewhere, it is screened by electrons. With a hydrogen bonding energy *E* in a lattice of about 1eV corresponding to $2 \cdot 10^{15}$ Hz (E =

$\hbar\omega$), the phonon frequency of $2 \cdot 10^{13}$ Hz corresponds to a potential change on a vacancy of 10^{-2} V. Integrating equation (1) over one cycle of phonon oscillation, the final formula for energy transfer to the nucleus with dependence on time is:

$$E(\tau) = e_o \frac{Q\omega}{6\pi} \frac{\partial^2 \varphi}{\partial x^2} \cdot \tau \ , \quad (2)$$

where Q is the quadrupole moment, ω is the phonon frequency, e_o is the elementary charge, φ is the potential at the nucleus location, and τ is the time. This is summarized in the table below, where ΔE is the energy transfer in one phonon oscillation, $\frac{\partial E}{\partial \tau}$ is the energy transfer rate, and T is the time (in seconds) required to transfer 10 MeV (for ^{105}Pd isotope).

TABLE 6

ω, MHz	ΔE, eV	$\frac{\partial E}{\partial \tau}$, eV/sec	T, S
10^{10}	10^{-11}	10^{-1}	10^{8}
10^{11}	10^{-10}	10	10^{6}
10^{12}	10^{-9}	10^{3}	10^{4}
10^{13}	10^{-8}	10^{5}	10^{2}
10^{14}	10^{-7}	10^{7}	1

This approach does not depend on the deformational energy of the nucleus, and the nucleus is a slow system, since the nucleus is "soft" to electric effects and the nucleus "oscillation" frequency (quadrupole) is less than 10^{13} Hz at energies below at least 5 MeV. This approach can be repeated infinitely, or until the quadrupole is simply pulled apart.

The nuclear "oscillation" time constant depends on the type of excitation. Gamma-emitting dipole nuclear transitions have a very short time of 10^{-12} - 10^{-20} s, quadrupole of 10^{-1} - 10^{-13}s, and octupole of a few hours for a 100 KeV excitation.

Gamma emission cannot occur with the proposed excitation, as well as beta-emission as explained hereafter. Alpha-emission is an inherently slow process (at least minutes) and it ensures the correctness of a slow nuclear system assumption.

The limitations of this approach are not clear. However, it appears valid at least with respect to the nucleon bonding energy, which is 5-10 MeV for heavy nuclei.

The given approach is entirely classical. In terms of the energy levels of a real nucleus, the nuclear ground level is split in the first cycle to about 10^{-10} eV, and the second cycle builds another 10^{-10} eV to this split level, and so forth (See energy relaxation section discussed hereafter). In this manner, virtual quantum levels are obtained and continue to build by splitting until energy transfer-in is stopped or the nucleus relaxation occurs. As the spin S during this process remains constant, gamma-radiation with this kind of nuclear excitation is completely suppressed.

At a phonon frequency of about 10^{13} Hz, the energy accumulation is obtained at a rate of 10^3 - 10^4 eV/s, or energy transfers of MeV-type energy corresponding to nuclear reactions can be reached in 10^2-10^3 seconds.

On the basis of energy portions that are transferred to the nucleus, it is possible to calculate the magnetic field required to maintain orientational stability. As the quadrupole is distorted, there is a possibility for the energy to go into rotational degrees of freedom. The evident condition is that the magnetic interaction energy must always be larger than the transferred energy.

Using the approach described in Wert, C., et al., *Physics of Solids*, (McGraw Hill, NY, 1970), pp. 477-479, the magnetic interaction energy is as follows: $\Delta E_H = g\mu_o\mu H_o$, where g is the splitting factor (normally from 2 to 6), μ_o is the nuclear magneton, μ is the magnetic permeability of the material, and H_o is the magnetic field. Estimations for the condition where $\Delta E_H > \Delta E_Q$ give a value for $H_o$min at approximately 50 Gauss for ^{105}Pd and approximately 20 gauss for ^{181}Ta. (at $\omega = 10^{14}$ Hz). The realistic phonon frequency is lower, thereby bringing the required magnetic field values within the earth magnetic field values.

An excitation rate lower than 10^{-8} eV per cycle guarantees that the lowest possible nuclear ground state will be excited first. With continuing excitation, the energy will go to the next level in a laser-pump fashion and move up the ladder. The

only remaining means for quick relaxation is through the electron system. This process is random, since an electron in resonance after an interaction with a nuclear level loses its resonance. The probability of such an event is relatively low because in a two particle interaction the conservation laws are severe. A nucleus excited in this manner will relax itself either back through the phonon resonance, spin resonance, and/or through the electrons, if the phonon resonance is terminated prior to alpha decay - fission. Depending on the excitation level, electron relaxation can take the form of photons (IR, optical, UV, etc.) or x-rays and Auger electrons at high excitations.

Optimal phonon frequencies for each potential element are not presently known. However, from a practicing point of view, this problem can readily be avoided by creating a broad band phonon resonator and exciting it, which eliminates the need for knowing the exact optimal frequencies for a specific element. Forming a broad band phonon resonator and sustaining the resonance by maintaining a high phonon density is the main objective of the present invention.

Summarizing the main principles of this invention, to effectuate an efficient energy transfer from the solid state lattice to the nuclear ground level, a two or more component lattice must be formed, with one sublattice consisting of atoms with pronounced mass difference from the other, at least one sublattice consisting of atoms having nuclei with pronounced quadrupole moment, a vacancy in one sublattice, and the conditions for a broad-band phonon resonance must be created and sustained, meaning that the resonator will amplify every single possible phonon mode selective phonon resonance is possible but not practical. For Pd, Ni, Ta and other cubic lattices having l-valent metal from pure geometrical considerations, the optimum hydrogen vacancy concentration is 12.5%. The concentration varies for other types of lattices, i.e., it is 6.25% for 2-valent metals, or approximately 4% for 3-valent.

Proposed Nuclear Reaction Model/Theory

The proposed nuclear excitation model is entirely different from anything presently known. Conventional energy transfer occurs at large energy portions, thereby allowing for energy relaxation on unoccupied energy levels. With a slow

excitation the spin is not affected, thus, forbidding energy relaxation in the form of gamma-emissions. In addition to regular selection rules based on the conservation of energy, momentum, spin and parity, this kind of excitation probably has additional selection rules. One possible additional selection rule is stable nuclear reaction products, because both the initial and final states have ample time under the present invention to form a stable nuclear shell which corresponds to the energy minimum within a common quantum state. Even without introducing new selection rules, of eighty elements with quadrupole moment only four, namely Re, Pm, In, and Mo allow energy release (positive Q reactions) with beta-decay. However, all beta-decays for the previous list of isotopes are forbidden by both the Fermi and Gamov-Teller selection rules. Thus beta-decay is forbidden.

Alpha decay and fission is allowed in some cases, sometimes even with positive Q, for example:

105Pd	→	17O + 88Sr +0.311 MeV (778.2)
105Pd	→	25Mg+ 80Se +2.539 MeV (359.7)
147Sm	→	4He+143Nd +2.323 MeV (34.6)
149Sm	→	4He+145Nd +1.868 MeV (41.1)
149Sm	→	11B +138La +0.713 MeV (381.5)
151Eu	→	14N +137Ba+10.199 MeV (92.9)
151Eu	→	27Al+124Sn+30.771 MeV (81.1)
159Tb	→	23Na+136Xe+26.402 MeV (78.2)
161Dy	→	25Mg+136Xe+31.542 MeV (75.6)
197Au	→	4He+193Ir +0.958 MeV (87.6)

Alpha decay is known to be very sensitive to external excitation. For example, the addition of only a few KeV to a 235 U nucleus, which is an extremely small energy compared to the nuclear barrier height, changes the alpha-decay rate dramatically. The same is probably true for alpha-decay in the present invention. The situation with fission is less clear and the experimental data for fission of "light" ($z<90$) elements is presently not conclusive. Thus, results for fission given here are speculative. The barrier exponential factor for alpha-decay is shown in parenthesis. For reactions not producing ^{4}He, the barrier exponential factor should be disregarded.

Overall, there are only six elements listed above that can produce reactions with positive energy release for both alpha decay and fission, with resulting stable isotopes.

Most of the allowed alpha-decays are with negative Q, but still can occur, since the energy transfer can be large enough. Examples of negative Q reactions with stable isotope products are as follows:

61Ni → 6Li+ 55Mn-20.596 MeV (22313.6)
61Ni → 8Be+ 53Cr-13.879 MeV (31290.6)
61Ni → 9Be+ 52Cr-20.153 MeV (33797.5)
63Cu → 6Li+ 57Fe-19.487 MeV (23206.4)
63Cu → 7Li+ 56Fe-19.886 MeV (25421.2)
63Cu → 10B + 53Cr-22.348 MeV (45167.7)
63Cu → 11B + 52Cr-18.834 MeV (47907.4)
65Cu → 7Li+ 58Fe-20.018 MeV (25421.1)
65Cu → 11B + 54Cr-18.997 MeV (47907.3)
67Zn → 2H + 65Cu-13.754 MeV (3856.4)
69Ga → 2H + 67Zn-14.578 MeV (3989.5)
69Ga → He+ 65Cu -4.486 MeV (13364.5)
69Ga → 7Li+ 62Ni-17.484 MeV (27377.4)
69Ga → 11B + 58Fe-15.838 MeV (51900.9)
71Ga → 7Li+ 64Ni-17.950 MeV (27377.3)
75As → 4He+ 71Ga -5.317 MeV (14286.6)
75As → 7Li+ 68Zn-17.935 MeV (29333.5)
75As → 11B + 64Ni-14.602 MeV (55894.4)
79Br → 2H + 77Se-14.607 MeV (4521.7)
79Br → 4He+ 75As -5.466 MeV (15208.7)
79Br → 7Li+ 72Ge-18.390 MeV (31289.8)
79Br → 8Be+ 71Ga-10.876 MeV (43658.8)
79Br → 11B + 68Zn-14.737 MeV (59888.0)
81Br → 7Li+ 74Ge-19.463 MeV (31289.7)
81Br → 11B + 70Zn-17.082 MeV (59887.9)
87Rb → 7Li+ 80Se-21.737 MeV (33246.0)
87Rb → 11B + 76Ge-20.046 MeV (63881.5)
87Sr → 4He+ 83Kr -7.321 MeV (16591.8)
91Zr → 17O + 74Ge-13.661 MeV (122858.2)
95Mo → 4He+ 91Zr -2.247 MeV (18436.1)
95Mo → 17O + 78Se -9.880 MeV (130538.6)
95Mo → 25Mg+ 70Zn -4.959 MeV (203313.3)
97Mo → 17O + 80Se -8.971 MeV (135466.1)
99Ru → 2He+ 97Mo-14.578 MeV (11176.8)
99Ru → 4He+ 95Mo -2.332 MeV (19358.3)
99Ru → 8Be+ 91Zr -4.672 MeV (56338.1)
99Ru → 17O + 82Kr -6.220 MeV (143436.8)
99Ru → 25Mg+ 74Ge -1.007 MeV (216870.4)
101Ru → 4He+ 97Mo -2.837 MeV (19358.3)
101Ru → 17O + 84Kr -4.714 MeV (143436.6)
101Ru → 25Mg+ 76Ge -1.548 MeV (216870.1)
105Pd → 4He+101Ru -2.887 MeV (20280.4)

105Pd	→	8Be+ 97Mo -5.816 MeV	(59155.7)
135Ba	→	4He+131Xe -1.870 MeV	(24891.2)
141Pr	→	6Li+135Ba-12.253 MeV	(49994.7)
145Nd	→	7Li+138La -9.819 MeV	(55744.4)
147Sm	→	2He+145Nd-12.325 MeV	(15968.6)
155Gd	→	9Be+146Nd -2.493 MeV	(90350.3)
157Gd	→	9Be+148Nd -4.767 MeV	(90350.2)
161Dy	→	2H +159Tb-11.658 MeV	(8647.0)
165Ho	→	2H +163Dy-11.658 MeV	(8780.0)
181Ta	→	2H +179Hf-11.103 MeV	(9578.6)
189Os	→	9Be+180Hf -0.545 MeV	(108424.7)
201Hg	→	9Be+192Os -3.132 MeV	(114449.5)

A paradoxal situation exists with isotopes for which all three channels (alpha, beta and gamma) are forbidden. Such a nucleus will be forced into multi-particle decay or fission. Multi-particle decay can explain certain tritium observations, and fission can explain production of stable isotopes. Fission can also compete with high negative Q alpha-decay, for example: $^{105}Pd_{46} \rightarrow {}^{25}Mg_{12} + {}^{80}Se_{34} + 2.53$ MeV. From barrier height considerations applicable in this case, this reaction is 10^3 - 10^4 times less probable than alpha-decay.

It must be noted, that all these reactions are extremely difficult to detect and special detectors are required, such as charge particle SSB detectors with partial coating on the surface and ionization chambers with samples inside. In the case of deuterides, 1W of power corresponds to a neutron flux from secondary d-d reactions resulting from the scattering of charged particles of less than 1 n/s, which is on the threshold of detection for most detectors.

For energy generation applications the first component of the two-component lattice must be capable of providing for a nuclear reaction with positive energy release and stable products (candidates listed previously). For element transmutation applications, the first component must have quadrupole moment and be capable of providing for a nuclear reaction with positive or negative energy release and stable products. For transmutation applications, the first component (heavy nuclei) comprises ^{61}Ni, $^{63,65}Cu$, ^{67}Zn, $^{69,71}Ga$, ^{75}As, $^{79,81}Br$, ^{85}Rb, ^{87}Sr, ^{91}Zr, $^{95,97}Mo$, $^{99,101}Ru$, ^{105}Pd, ^{135}Ba, ^{141}Pr, ^{145}Nd, $^{147,149}Sm$, ^{151}Eu, $^{155,157}Gd$, ^{159}Tb, ^{161}Dy, ^{165}Ho, ^{181}Ta, ^{189}Os, ^{197}Au, ^{201}Hg, or combinations thereof. For energy storage applications, the first

components listed above for energy generation and transmutation will suffice. However, the preferred elements for energy storage have a large quadrupole moment and do not exhibit positive or negative energy release.

Proposed Energy Relaxation Model

As discussed previously, there are only a few possibilities for relaxation of the energy transferred to the nucleus. If the transfer is fast and long enough, nuclear reaction-type relaxation results, such as alpha-decay or fission.

When Anderson's localization theorem is not fulfilled, a random coupling from the phonon to the nuclear quadrupole exists, which in the absence of a magnetic field provides nuclear levels with about 10^{-9} - 10^{-8} eV spacing: $E = \frac{e^2qQ}{4I(2I-1)}$, where e is the elementary charge, q is the electric field gradient, Q is the nuclear quadrupole moment, and I is the spin (*See* Bolef et al., *Nuclear Acoustic Resonance*, pp. 12, 88). The number of levels are I + ½.

When Anderson's condition is fulfilled, a slow nuclear system exists in which theenergy is transferred at a rate much faster than it can relax. As a result, the virtual energy levels associated with this process follow the relation: $E = \frac{e^2qQ}{4\pi I(2I-1)} \cdot N$ (N= $\pm$1,$\pm$2, ...) Quantum number N is the integer part of $\omega\tau$, where ω is the phonon frequency and τ is the time. Since the "quantum number" N is time dependent, it represents the virtual energy levels. The total number of virtual quantum levels introduced by the energy transfer for isotopes with spin I=5/2 will be $3 \cdot N$. In the presence of a magnetic field and when degeneracy is removed, the number of levels will be $6 \cdot N$. Hence, a phonon frequency of about 10^{13} Hz after 10 seconds of exposition results in about 10^{15} energy levels. Assuming interruption of a resonant phonon mode and that the total transferred energy is less than that required for nuclear reactions, it must be relaxed to the initial situation, which corresponds to the random phonon mode.

From classical considerations, the electric field induced by the nuclear quadrupole at a vacancy location is 10^5 times weaker than that induced by an oscillating charge dipole at a nuclear location with a corresponding transfer time of about 10^4 s. In reality, to de-excite one single level (I=s/2) the following condition must be met:

$$3/20\ e^2aQ = \hbar\omega_o\ (n+1/2),$$

where ω is the frequency of lattice phonons, $\hbar$ is Plank's constant and n is the quantum number for dipole oscillation. Even for $n= 0$, ω_o corresponds to 10^7 - 10^8 Hz. This is a very low frequency region even for acoustic phonons. Moreover, the density of the states in this region is typically low. If the lattice is not in thermal equilibrium, decay of higher frequency phonons can populate this frequency region and a relaxation time comparable with 10^4 s results. In other words, application of a thermal gradient allows the stored energy to be retrieved.

Yet another possibility for de-excitation of levels is spin-quadrupole relaxation, which is one of the main fields in nuclear acoustic resonance (*See* Bolef, D., et al., *Nuclear Acoustic Resonance*, pp. 183-192). This method can provide relaxation rates comparable with quadrupole-phonon relaxation, but requires a strong oscillating magnetic field.

In summary, the method and apparatus disclosed herein is a significant improvement from the present state of the art of energy generation from methods and apparatus storing light elements in heavy elements.

The invention may be embodied in other specific forms without departing from its spirit or essential characteristics. The described embodiments are to be considered in all respects only as illustrative and not restrictive. The scope of the invention is, therefore, indicated by the appended claims rather than by the foregoing description. All changes which come within the meaning and range of equivalency of the claims are to be embraced within their scope.

What is claimed is:

CLAIMS:

1. A method of generating energy comprising the steps of:

forming a lattice with two or more components capable of providing a sustained phonon resonance, wherein said lattice comprises a first and second component, said first component comprising elements having nuclei with quadrupole moment and from the group comprising Pd, Sm, Eu, Tb, Dy, Au, or combinations thereof, said second component comprising atoms having atomic charge less than the first component, having a different phonon spectrum than the first component and having vacancies in the lattice;

maintaining orientational stability of the nuclei of the first component; and

creating and sustaining a phonon resonance within the lattice having resonance frequency of about 10^{11} to about 10^{14} Hz, such that replenishment energy of the phonon resonance is greater than energy transfer to the first component.

2. A method defined in claim 1, wherein the creating and sustaining a phonon resonance step comprises applying a phonon flux to the lattice surface.

3. A method defined in claim 2, wherein the step of applying a phonon flux comprises creating a thermal gradient along the lattice.

4. A method defined in claim 3, wherein said thermal gradient creating step comprises applying an electron flux.

5. A method defined in claim 3, wherein said thermal gradient creating step comprises applying an acoustic flux.

6. A method defined in claim 3, wherein said thermal gradient creating step comprises applying a thermal diffusion flux.

7. A method defined in claim 3, wherein said thermal gradient creating step comprises applying an AC magnetic flux.

8. A method defined in claim 3, wherein said thermal gradient creating step comprises applying an electron beam.

9. A method defined in claim 3, wherein said thermal gradient creating step comprises applying an ion beam.

10. A method defined in claim 3, wherein said thermal gradient creating step comprises applying a plasma beam.

11. A method defined in claim 3, wherein said thermal gradient creating step comprises applying radio frequency electromagnetic radiation.

12. A method defined in claim 2, wherein the step of applying a phonon flux comprises applying a photon flux.

13. A method defined in claim 2, wherein the step of applying a phonon flux comprises applying microwave radiation.

14. A method defined in claim 1, wherein said second component comprises deuterium.

15. A method defined in claim 1, wherein said second component comprises hydrogen.

16. A method defined in claim 1, wherein said second component comprises lithium.

17. A method defined in claim 1, wherein said second component comprises beryllium.

18. A method defined in claim 1, wherein said second component comprises borides.

19. A method defined in claim 1, wherein said second component comprises nitrides.

20. A method defined in claim 1, wherein said second component comprises oxides.

21. A method defined in claim 1, wherein said second component comprises flourides.

22. A method defined in claim 1, wherein said second component comprises chlorides.

23. A method defined in claim 1, wherein said second component comprises halides.

24. A method defined in claim 1, wherein said second component comprises carbides.

25. A method defined in claim 1, wherein said second component comprises a combination of deuterium, hydrogen, lithium, beryllium, borides, nitrides, oxides, flourides, chlorides, halides, or carbides.

26. A device for generating energy comprising:

a lattice with two or more components capable of providing a sustained phonon resonance, wherein said lattice comprises a first and second component, said first component comprising elements having nuclei with quadrupole moment from the group comprising Pd, Sm, Eu, Tb, Dy, Au, or combinations thereof, said second component comprising atoms having atomic charge less than the first component, having a different

phonon spectrum than the first component and having stable charge vacancies in the lattice;

means for maintaining orientational stability of the nuclei of the first component; and

means for creating and sustaining a phonon resonance within the lattice having resonance frequency of about 10^{11} to about 10^{14} Hz, such that replenishment energy of the phonon resonance is greater than energy transfer to the first component.

27. A device defined in claim 26, wherein the second component comprises deuterium.

28. A device defined in claim 26, wherein the second component comprises hydrogen.

29. A device defined in claim 26, wherein the second component comprises lithium.

30. A device defined in claim 26, wherein the second component comprises beryllium.

31. A device defined in claim 26, wherein said second component comprises borides.

32. A device defined in claim 26, wherein said second component comprises nitrides.

33. A device defined in claim 26, wherein said second component comprises oxides.

34. A device defined in claim 26, wherein said second component comprises flourides.

35. A device defined in claim 26, wherein said second component comprises chlorides.

36. A device defined in claim 26, wherein said second component comprises halides.

37. A device defined in claim 26, wherein said second component comprises carbides.

38. A device defined in claim 26, wherein said second component comprises a combination of deuterium, hydrogen, lithium, beryllium, borides, nitrides, oxides, flourides, chlorides, halides, or carbides.

39. A device defined in claim 26, wherein said phonon resonance means comprises means for applying a phonon flux to the lattice surface.

40. A device defined in claim 39, wherein said phonon flux means comprises means for creating a thermal gradient along the lattice.

41. A device defined in claim 40, wherein the means for creating a thermal gradient comprises heat conducting contacts and the lattice includes one or more sides, said heat conducting contacts being disposed on said one or more sides.

42. A device defined in claim 40, wherein the means for creating a thermal gradient comprises a convective heat exchange means and the lattice includes one or more sides, said convective heat exchange means being disposed on said one or more sides.

43. A device defined in claim 40, wherein the means for creating a thermal gradient comprises an electron flux.

44. A device defined in claim 40, wherein the means for creating a thermal gradient comprises an acoustic flux.

45. A device defined in claim 40, wherein the means for creating a thermal gradient comprises a thermal diffusion flux.

46. A device defined in claim 40, wherein the means for creating a thermal gradient comprises an AC magnetic flux.

47. A device defined in claim 40, wherein the means for creating a thermal gradient comprises electron beam.

48. A device defined in claim 40, wherein the means for creating a thermal gradient comprises ion beam.

49. A device defined in claim 40, wherein the means for creating a thermal gradient comprises plasma beam.

50. A device defined in claim 40, wherein the means for creating a thermal gradient comprises radio frequency electromagnetic radiation.

51. A device defined in claim 39, wherein said phonon flux means comprises a photon flux.

52. A device defined in claim 39, wherein said phonon flux means comprises microwave radiation.

53. A device defined in claim 26, wherein said lattice includes a surface and said sustained phonon resonance occurs with reflections on said surface.

54. A device defined in claim 26, wherein said lattice includes a phonon reflecting surface and said sustained phonon resonance occurs with reflections inside the lattice.

55. A device defined in claim 26, wherein the first component comprises nuclei having spin of at least 1 nuclear magneton.

56. A device defined in claim 26, further comprising impurities in the lattice of one or more elements having spin of at least about 1 nuclear megnetons.

57. A device defined in claim 26, wherein the lattice is of spherical shape.

58. A device defined in claim 26, wherein the lattice is of elliptical shape.

59. A device defined in claim 26, wherein the lattice comprises crystallites having size of less than about 10^{-6} meters.

60. A device defined in claim 26, wherein the lattice comprises wires having a diameter of less than about 10^{-6} meters.

61. A device defined in claim 26, further comprising one or more reflecting layers for phonon reflection.

62. A device defined in claim 61, wherein the reflecting layer thickness is at least about three phonon wavelengths.

63. A device defined in claim 61, wherein the reflecting layer comprises Ta, Hf, Re, Os, or combinations thereof.

64. A device defined in claim 61, wherein the reflecting layer comprises a material having elastic constants different from that of the first and second components combined.

65. A device defined in claim 61, wherein the reflecting layer is deposited on the lattice.

66. A device defined in claim 26, wherein the first component comprises polycrystal material with average grain size of about 10^{-6}m at a phonon flux of about 10^{4}W/m^2, 10^{-5}m at 10^{5}W/m^2, or 10^{-4}m at 10^{6}W/m^2.

67. A device defined in claim 26, wherein the first component comprises single crystal material with distance, x, between phonon reflecting surfaces which follows the equation $x = 1/\alpha$, where α is phonon attenuation for a given material.

68. A device defined in claim 26, wherein the first component comprises single crystal material having crystallographic orientation <110> between phonon reflecting surfaces for materials with face-centered-cubic structures.

69. A device defined in claim 26, wherein the first component comprises single crystal material having crystallographic orientation <100> between phonon reflecting surfaces for materials with body-centered-cubic structures.

70. A device defined in claim 26, wherein the first component comprises single crystal material having crystallographic orientation <1000> (c-axis) between phonon reflecting surfaces for materials with hexagonal closely packed lattices.

71. A method of storing energy comprising the steps of:

forming a lattice with two or more components capable of providing a sustained phonon resonance, wherein lattice comprises a first and second component, said first component comprising elements having nuclei with quadrupole moment, said second

component comprising atoms having atomic charge less than the first component, having a different phonon spectrum than the first component and having vacancies in the lattice;

maintaining orientational stability of the nuclei of the first component; and

creating and sustaining a phonon resonance within the lattice having resonance frequency of about 10^{11} to about 10^{14} Hz, such that replenishment energy of the phonon resonance is greater than energy transfer to the first component.

72. A device for storing energy comprising:

a lattice with two or more components capable of providing a sustained phonon resonance, wherein said lattice comprises a first and second component, said first component comprising elements having nuclei with quadrupole moment, said second component comprising atoms having atomic charge less than the first component, having a different phonon spectrum than the first component and having vacancies in the lattice;

means for maintaining orientational stability of the nuclei of the first component; and

means for creating and sustaining a phonon resonance within the lattice having resonance frequency of about 10^{11} to about 10^{14} Hz, such that replenishment energy of the phonon resonance is greater than energy transfer to the first component.

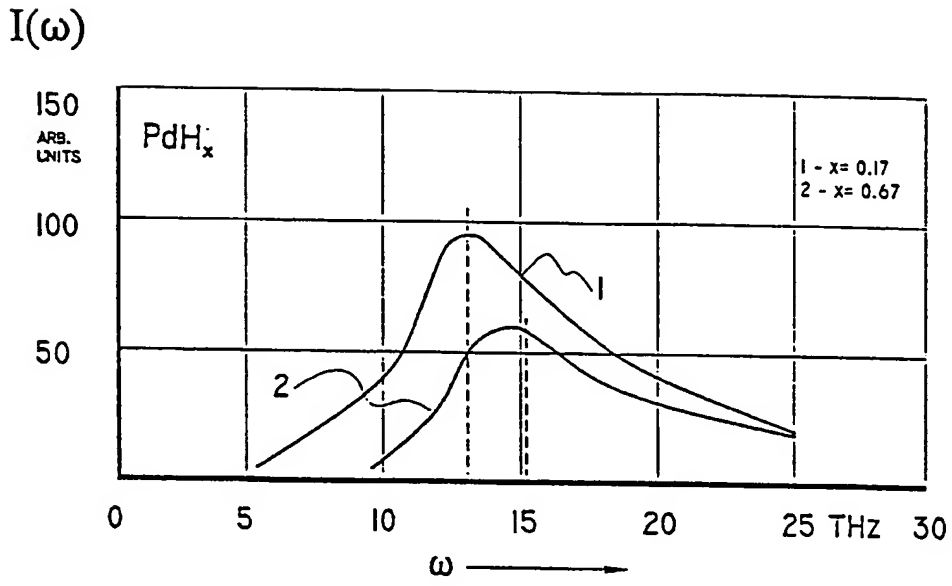
I(ω)
150
ARB. UNITS
100
50
PdH$_x$
1 - x= 0.17
2 - x= 0.67
1
2
0
5
10
15
20
25 THz
30
ω

FIG. 1

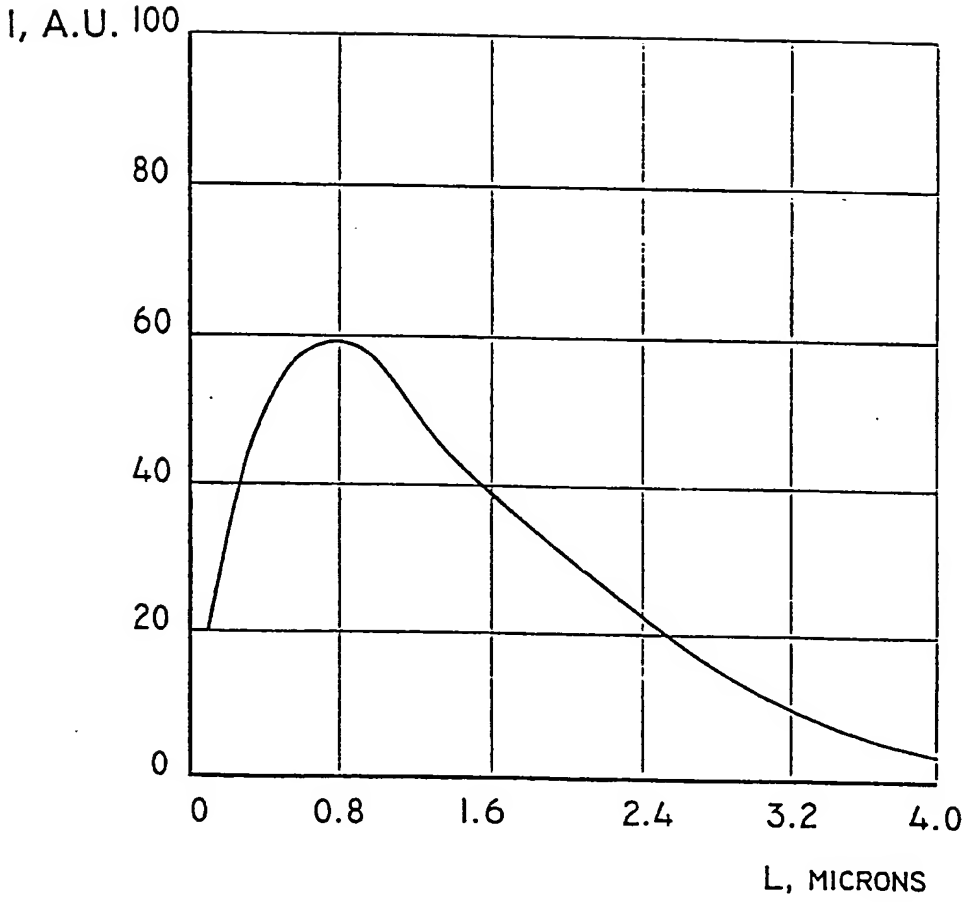

FIG. 2

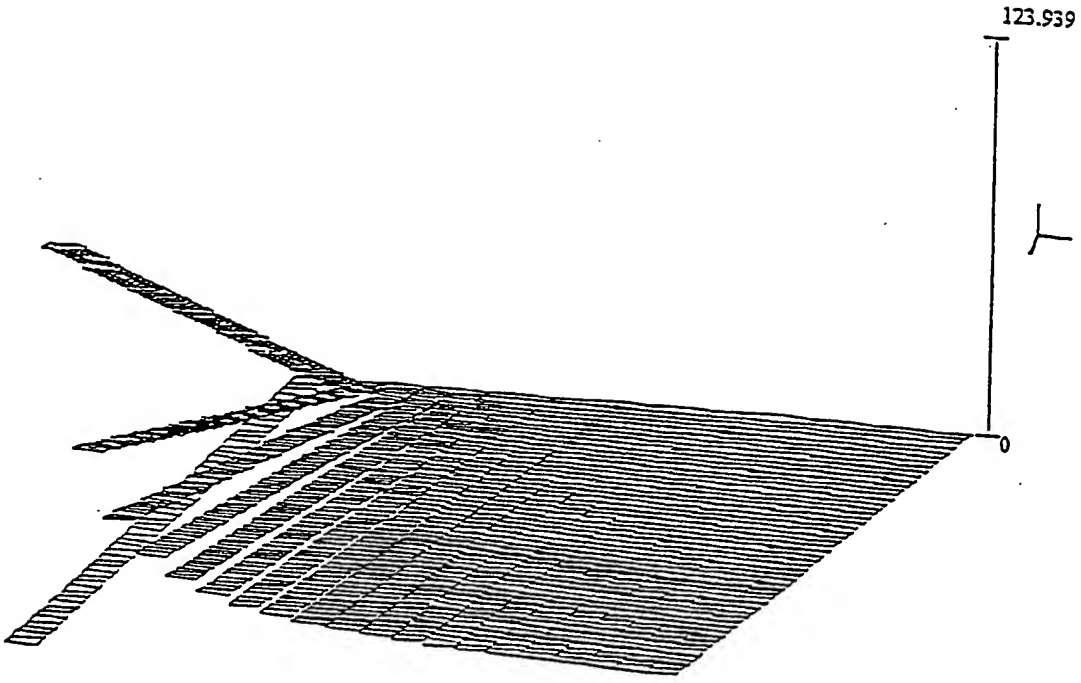

FIG. 3

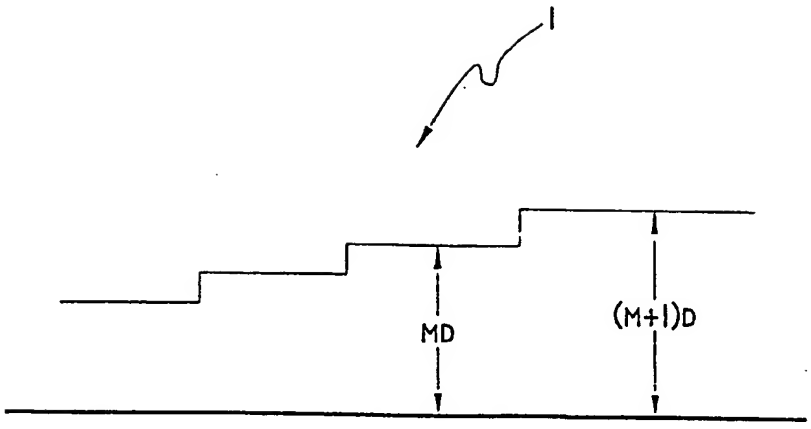

FIG. 4

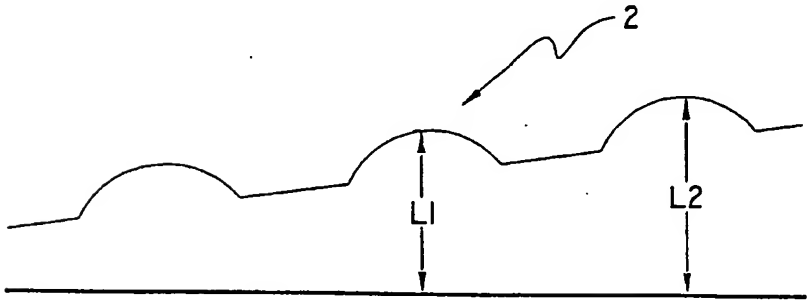

FIG. 5

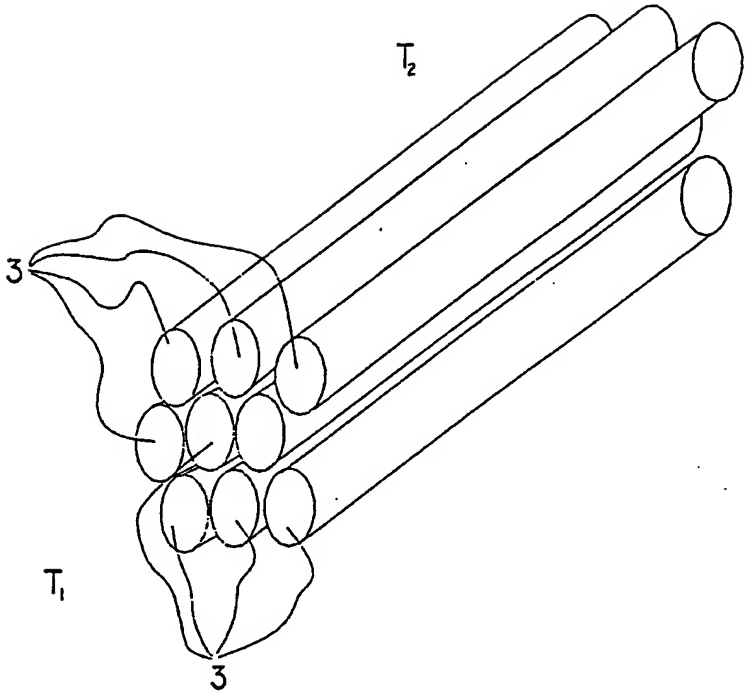

FIG. 6

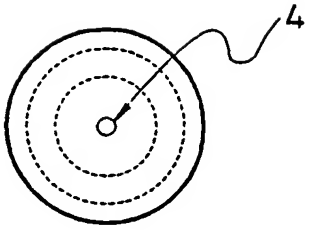

FIG. 7

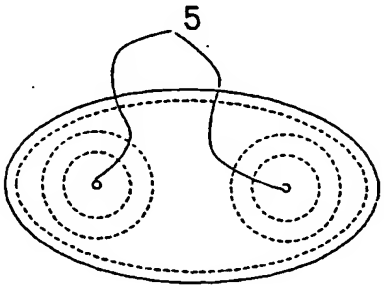

FIG. 8

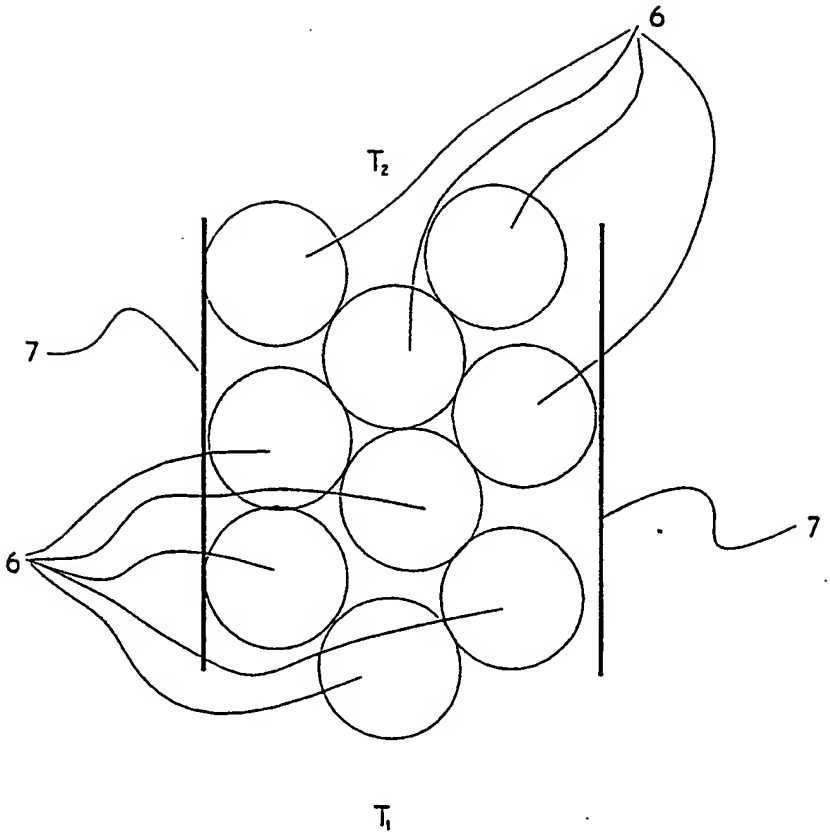

FIG. 9

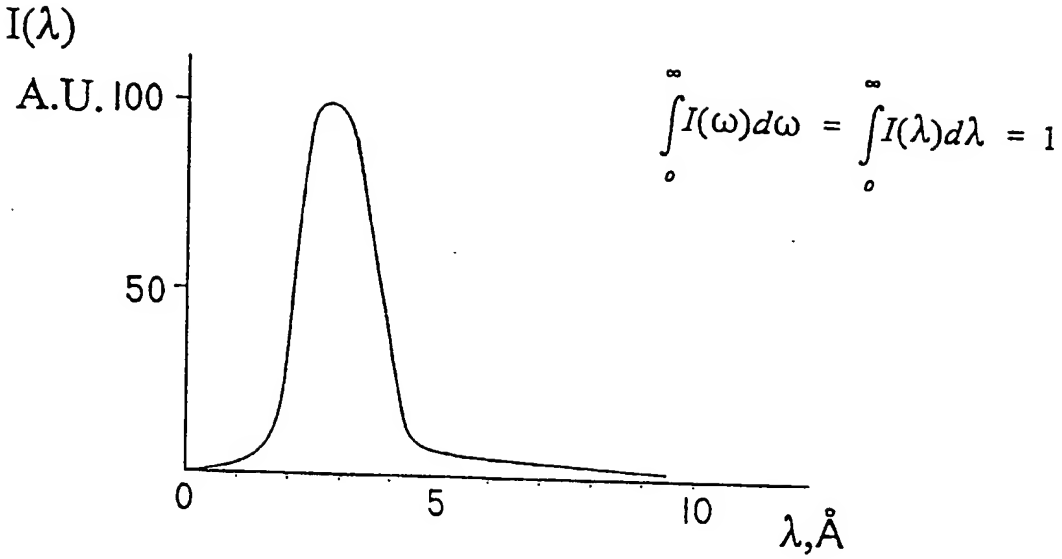

FIG. 10

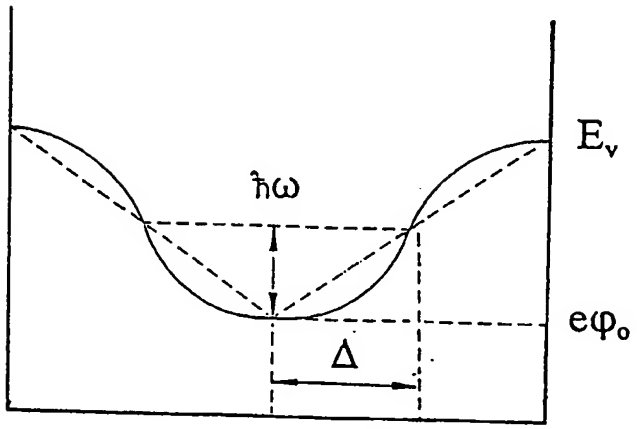

$$\Delta = \frac{d}{2}\frac{\hbar\omega}{E_v}$$

FIG. 11

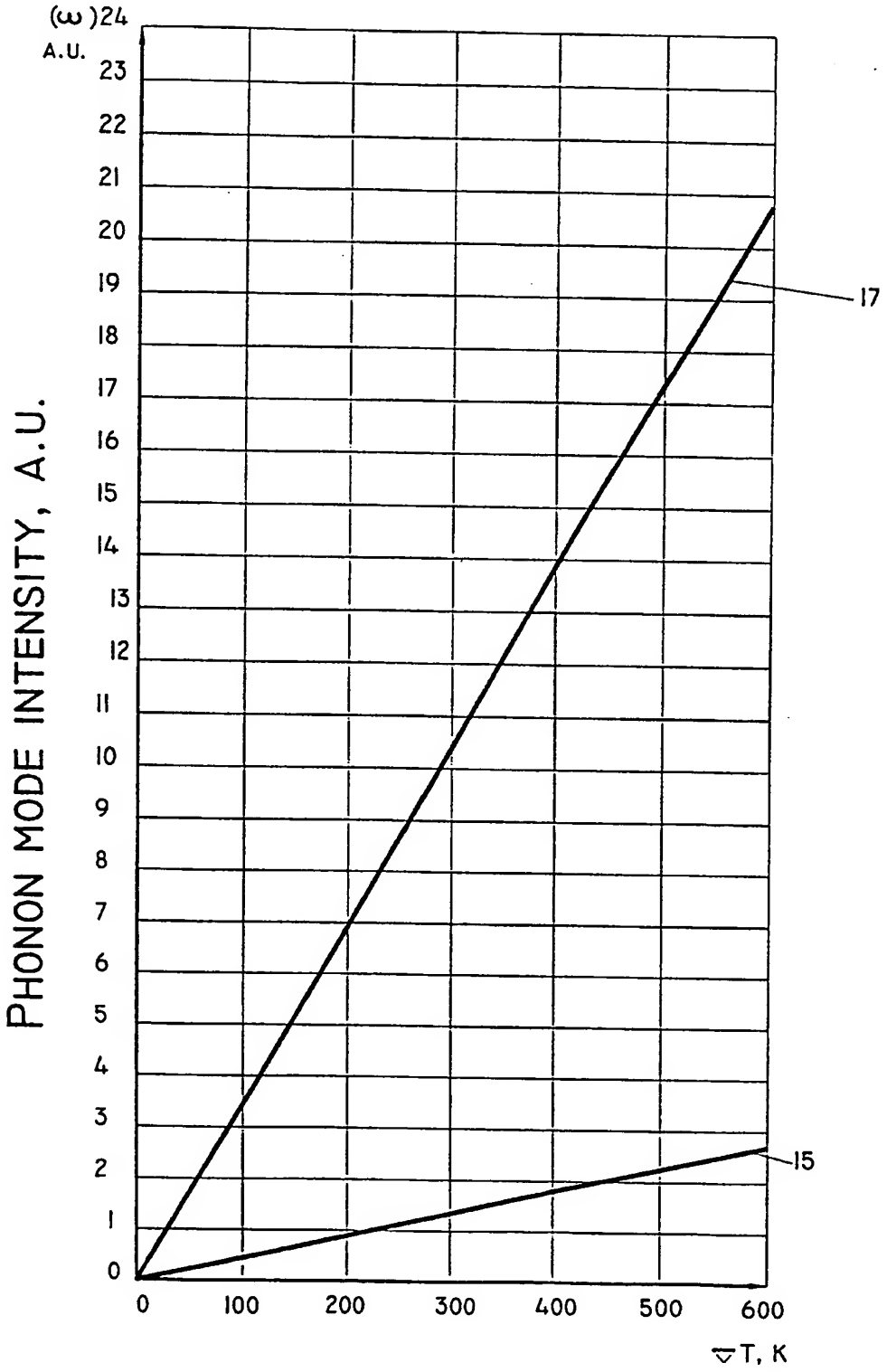
(ω)24
A.U.
23
22
21
20
19
18
17
16
15
14
13
12
11
10
9
8
7
6
5
4
3
2
1
0
PHONON MODE INTENSITY, A.U.
17
15
0
100
200
300
400
500
600
T, K

FIG. 12

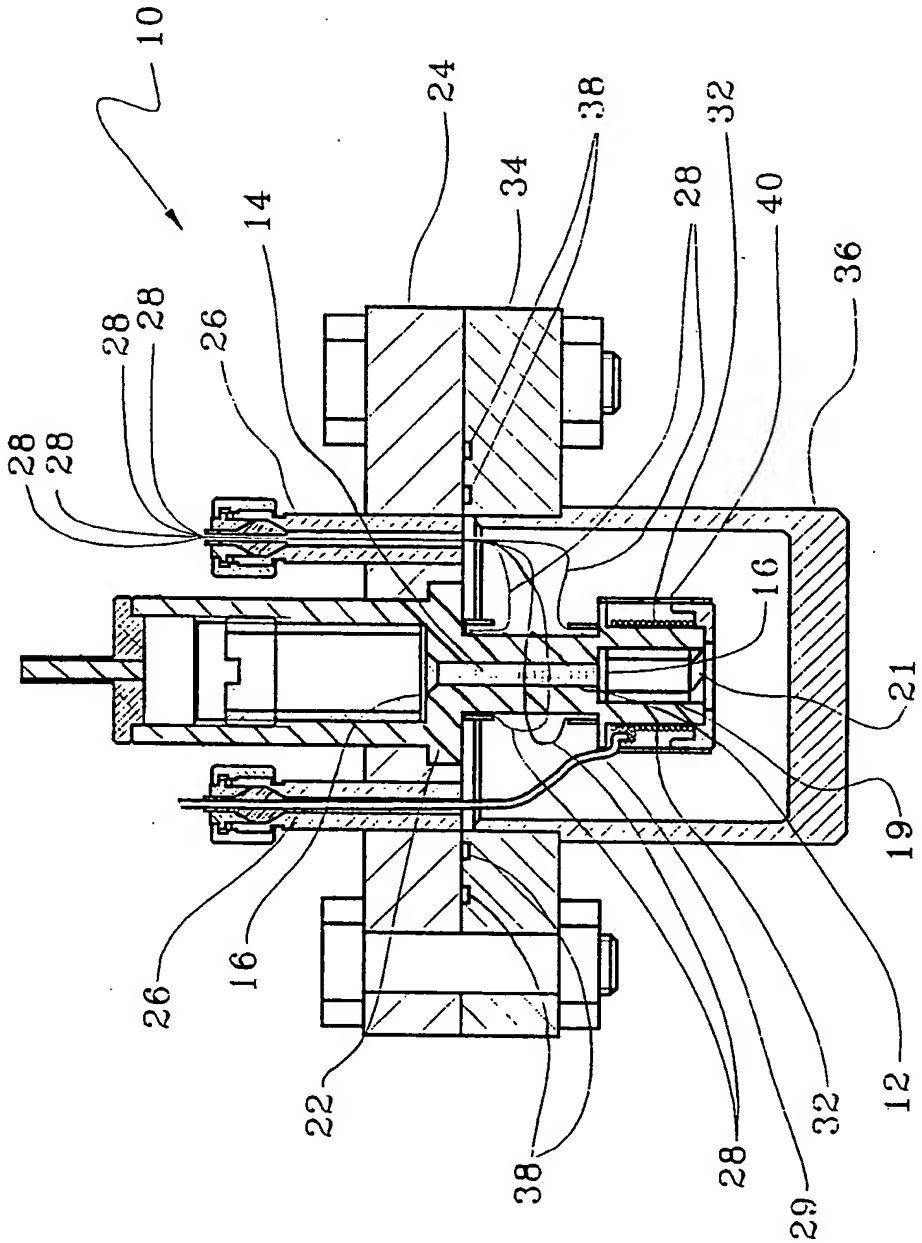
10
24
38
32
34
28
40
14
36
28
28
26
28
28
16
21
19
26
16
22
38
28
32
29
12

FIG. 13

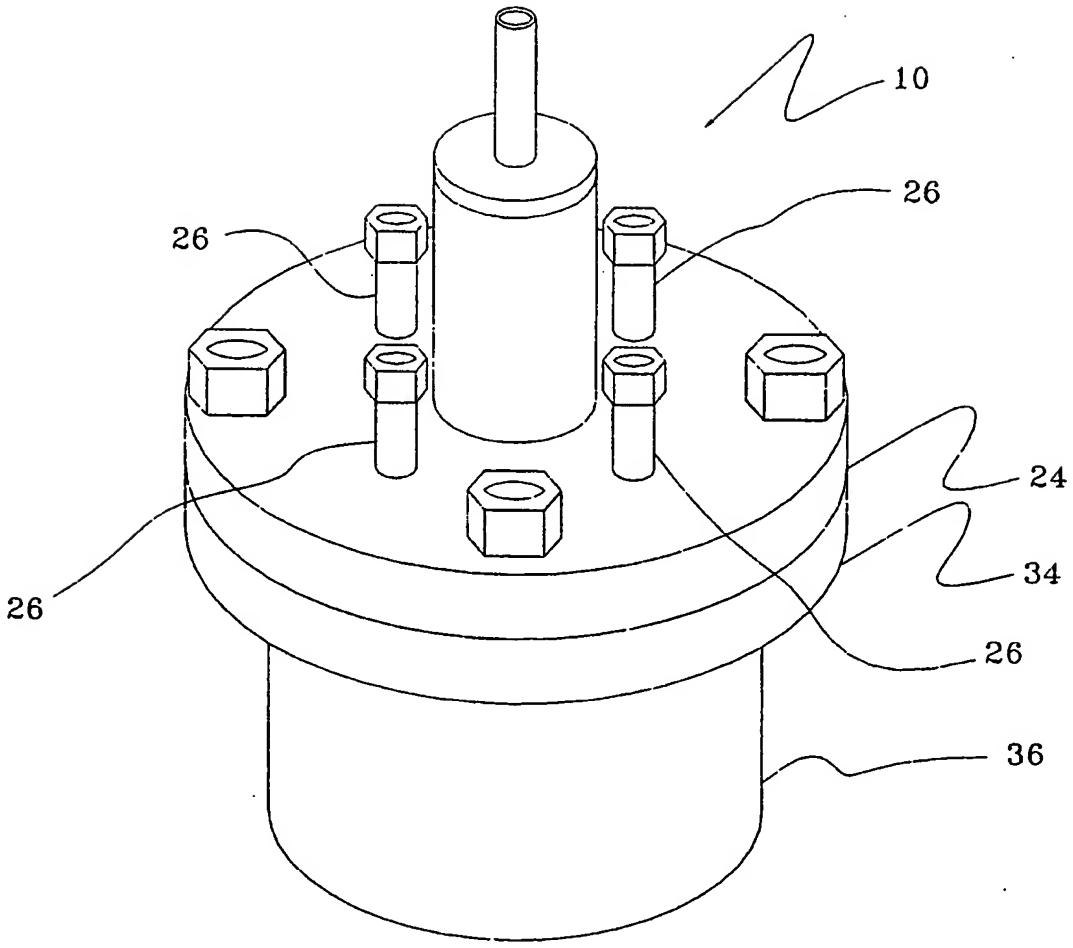

FIG. 14

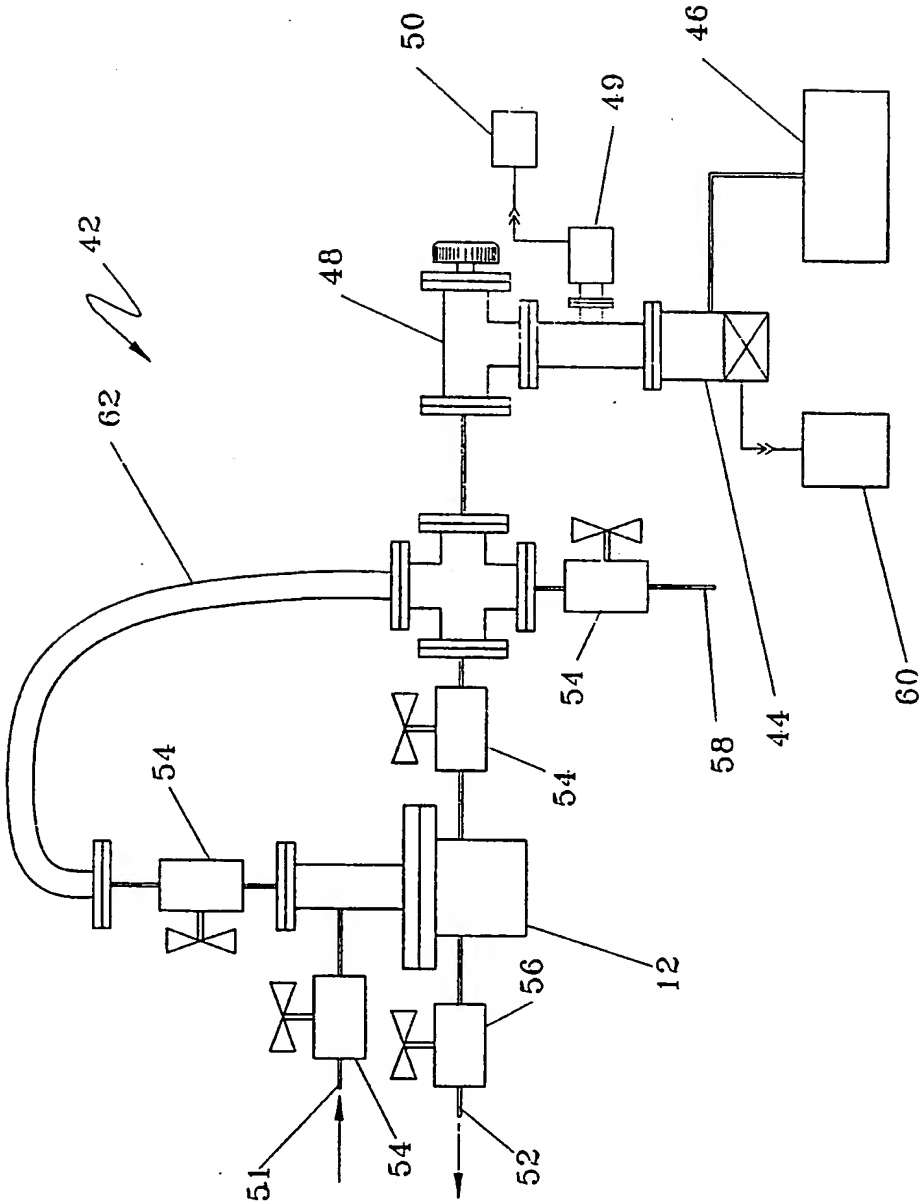

FIG. 15

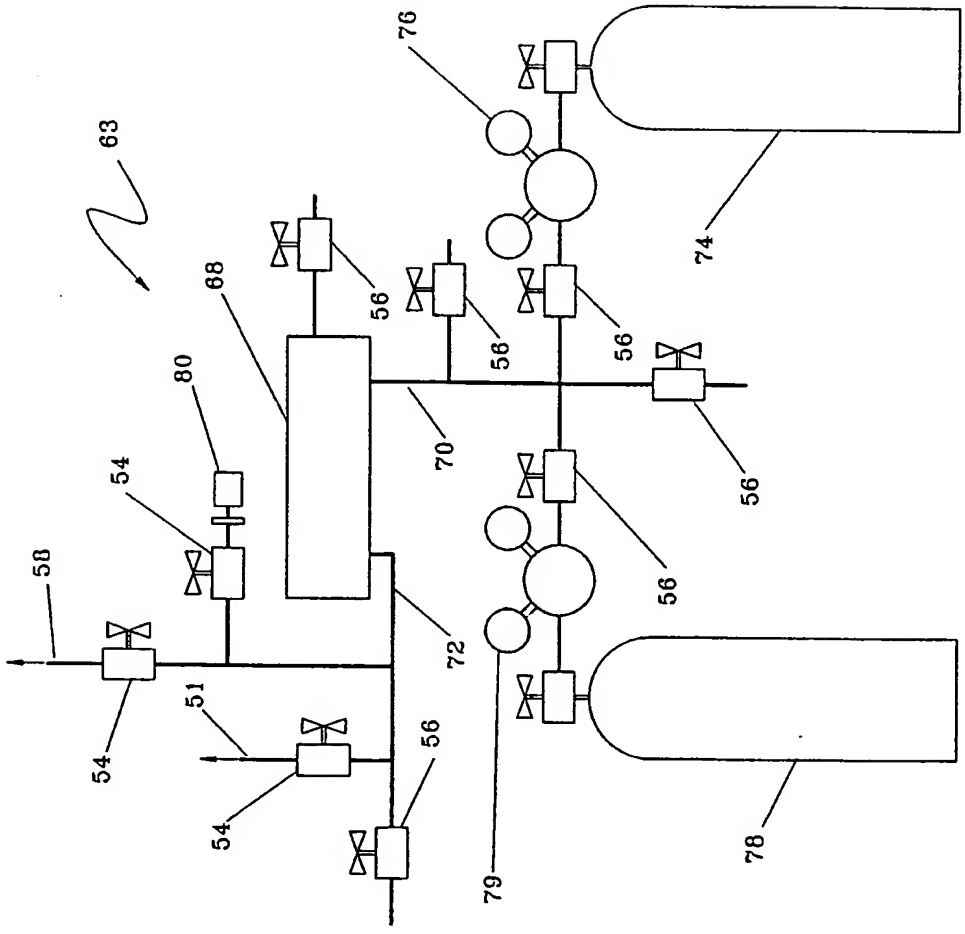

FIG. 16

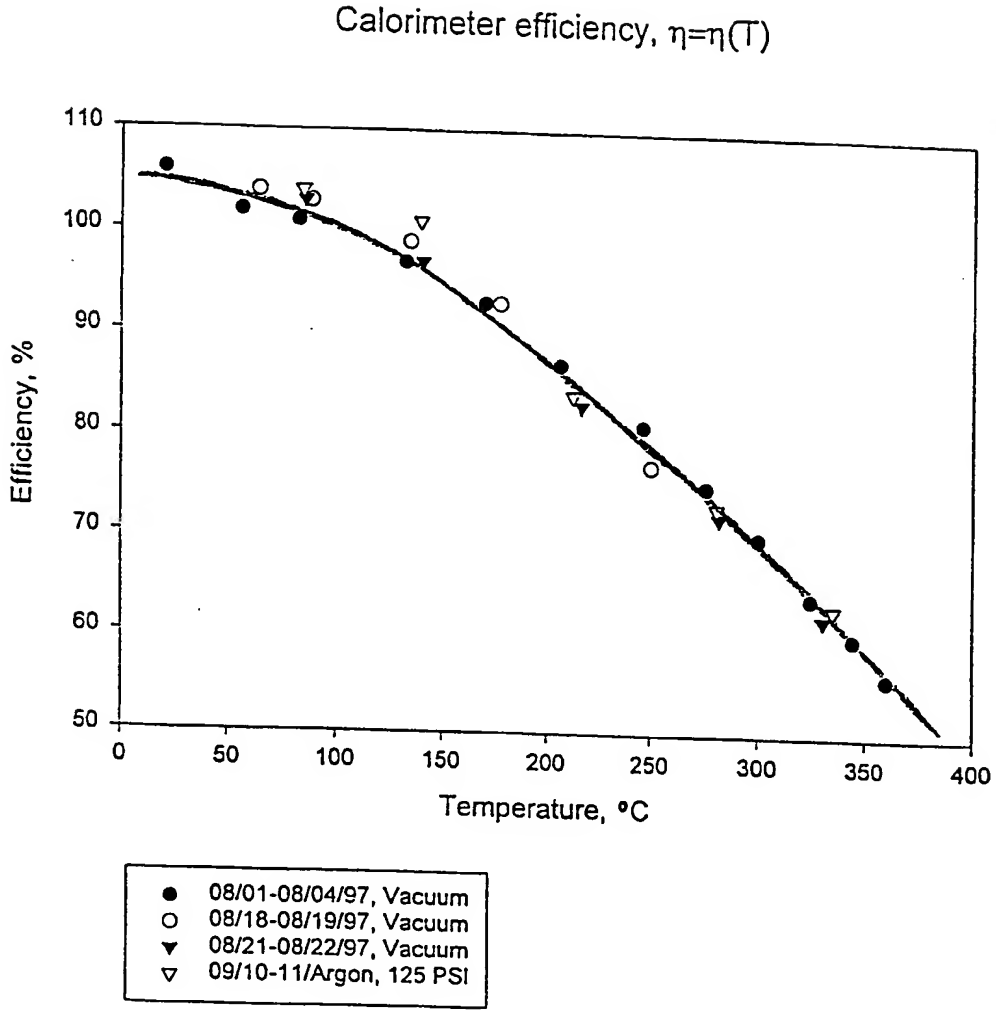
Calorimeter efficiency, η=η(T)
Efficiency, %
110
100
90
80
70
60
50
0
50
100
150
200
250
300
350
400
Temperature, °C
08/01-08/04/97, Vacuum
08/18-08/19/97, Vacuum
08/21-08/22/97, Vacuum
09/10-11/Argon, 125 PSI

FIG. 17

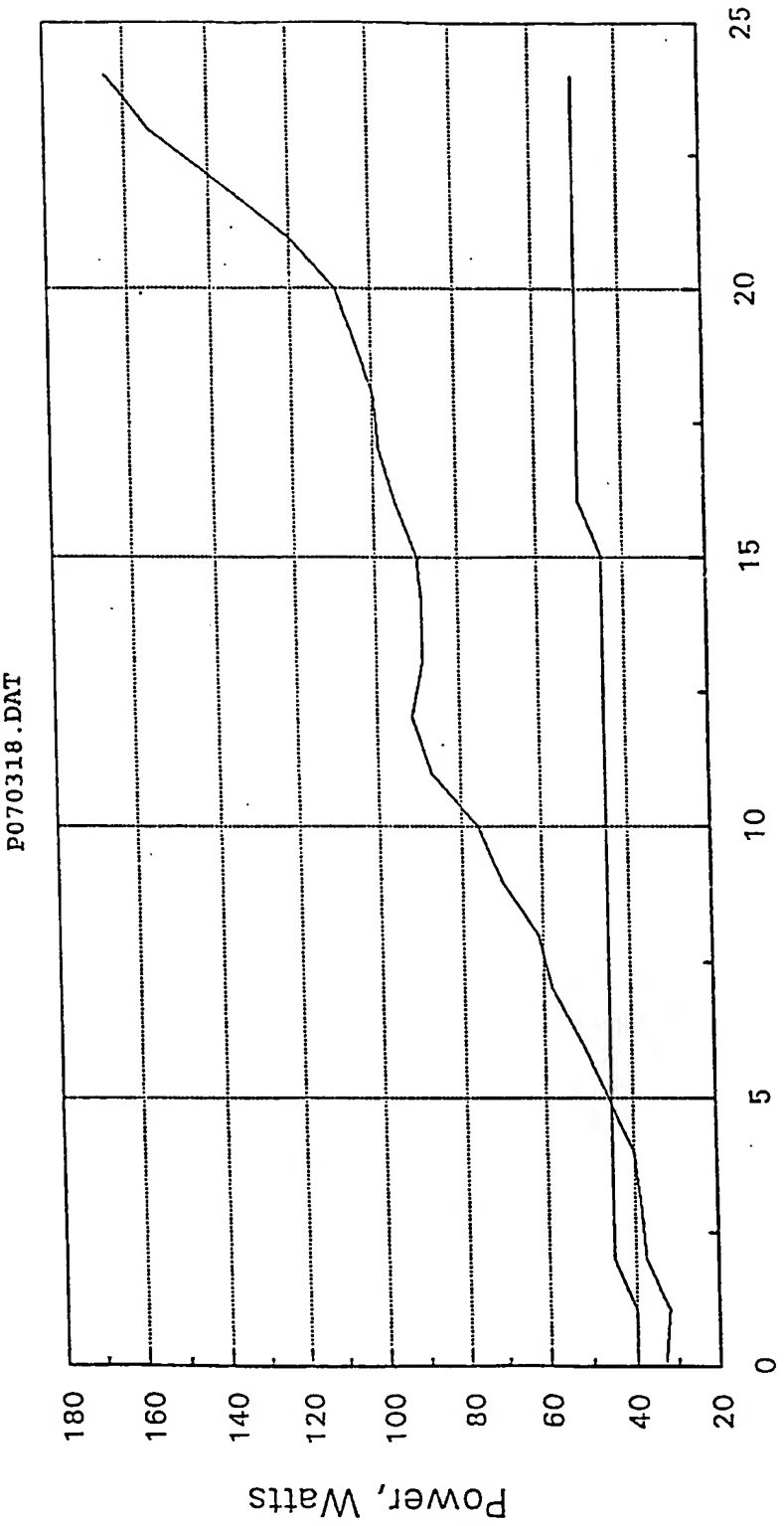
P070318.DAT
Power, Watts
180
160
140
120
100
80
60
40
20
0
5
10
15
20
25

FIG. 18

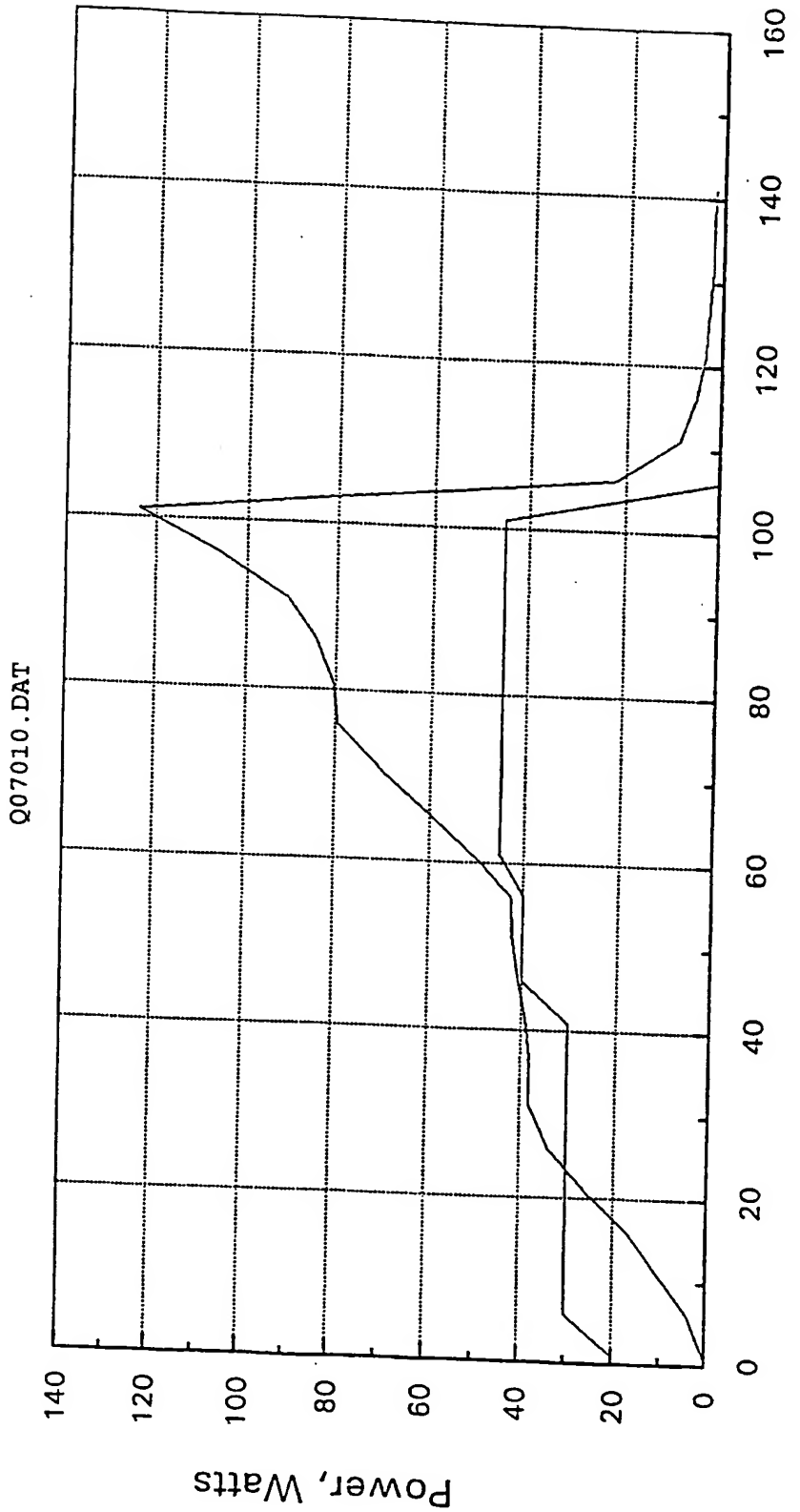

FIG. 19

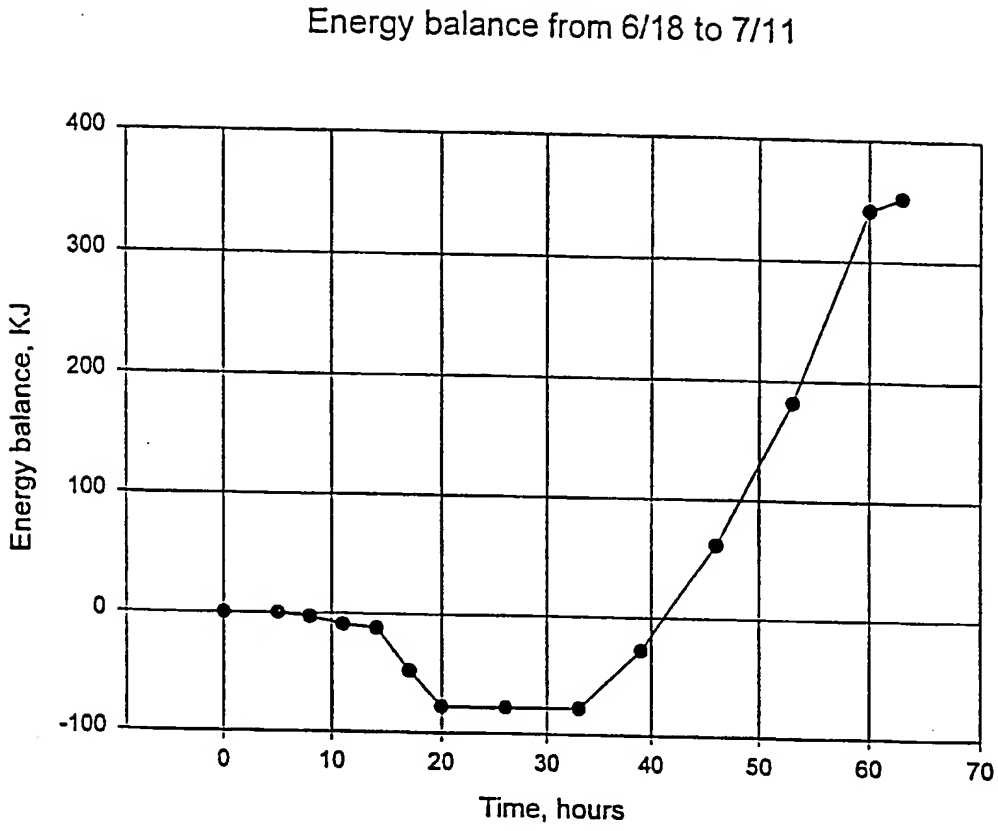
Energy balance from 6/18 to 7/11
Energy balance, KJ
400
300
200
100
0
-100
0
10
20
30
40
50
60
70
Time, hours

FIG. 20

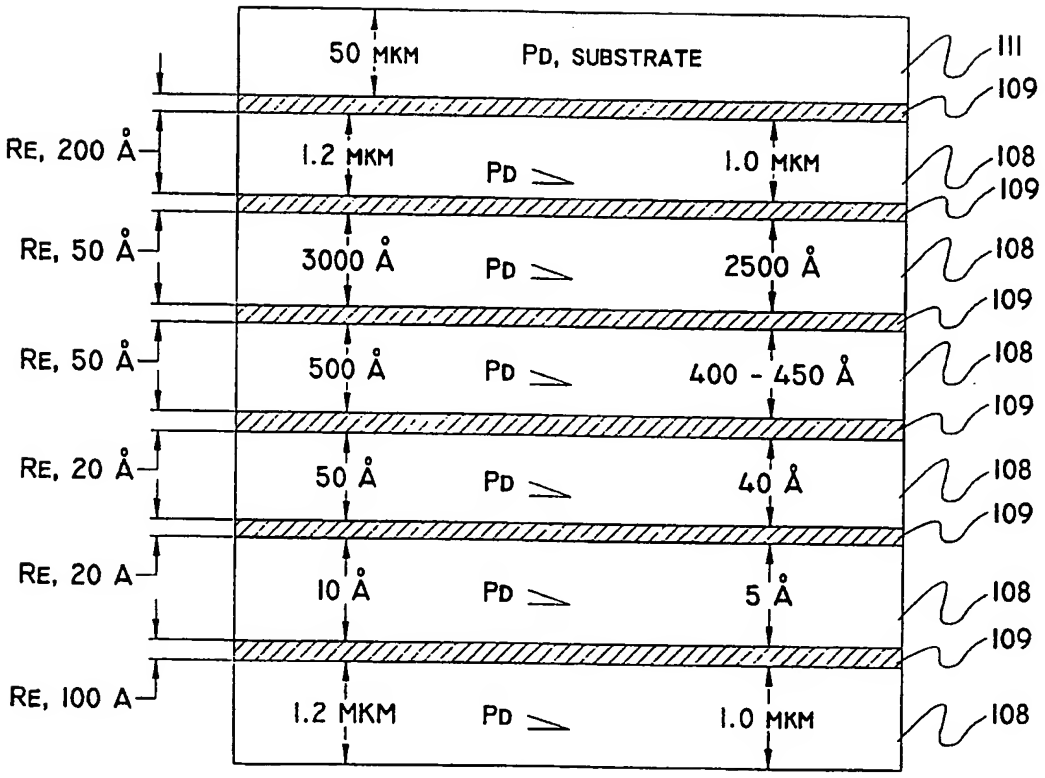
50 MKM
PD, SUBSTRATE
111
109
RE, 200 Å
1.2 MKM
PD
1.0 MKM
108
109
RE, 50 Å
3000 Å
PD
2500 Å
108
109
RE, 50 Å
500 Å
PD
400 - 450 Å
108
109
RE, 20 Å
50 Å
PD
40 Å
108
109
RE, 20 A
10 Å
PD
5 Å
108
109
RE, 100 A
1.2 MKM
PD
1.0 MKM
108

FIG. 21

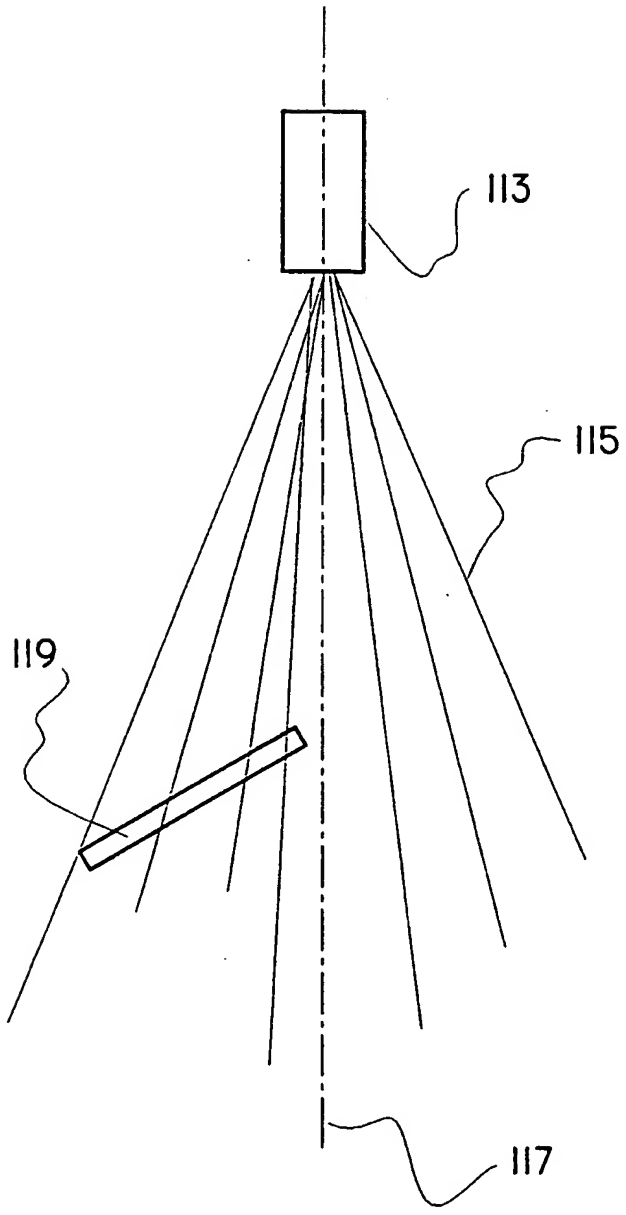

FIG. 22

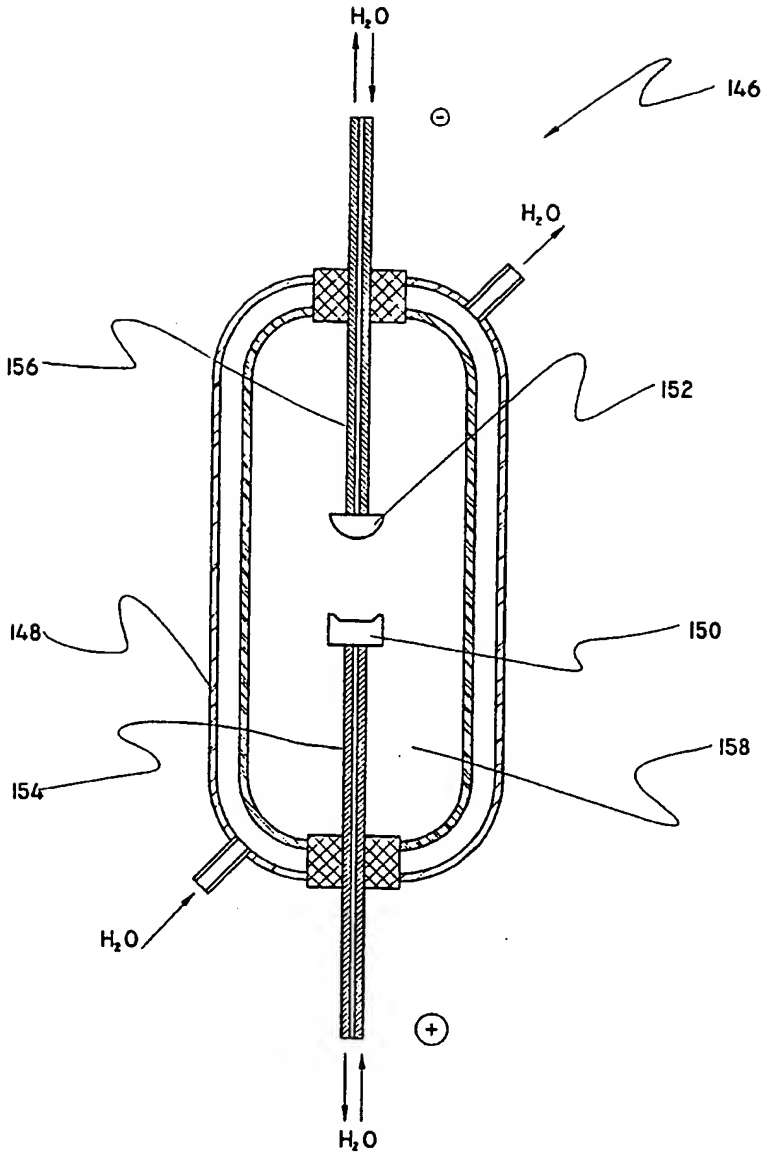

FIG. 23

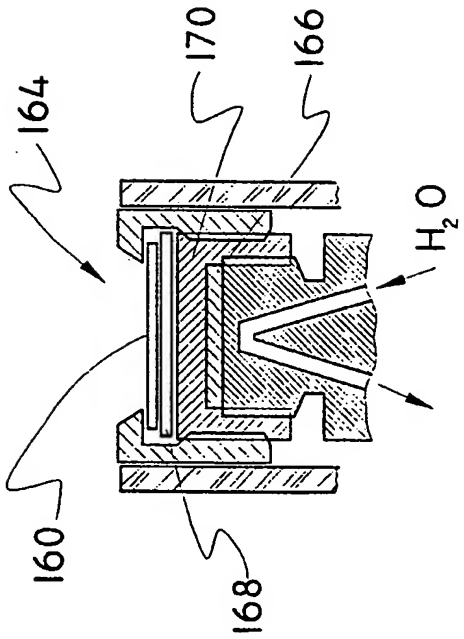

FIG. 25

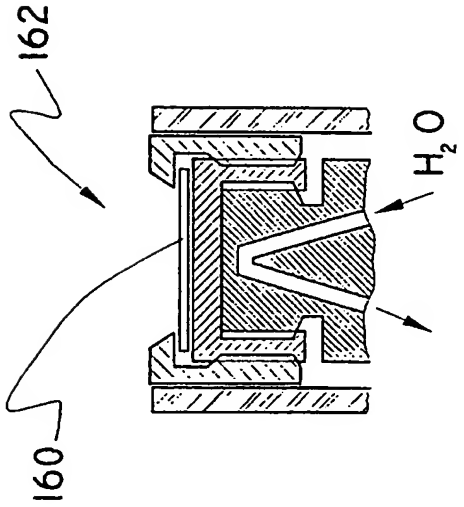

FIG. 24

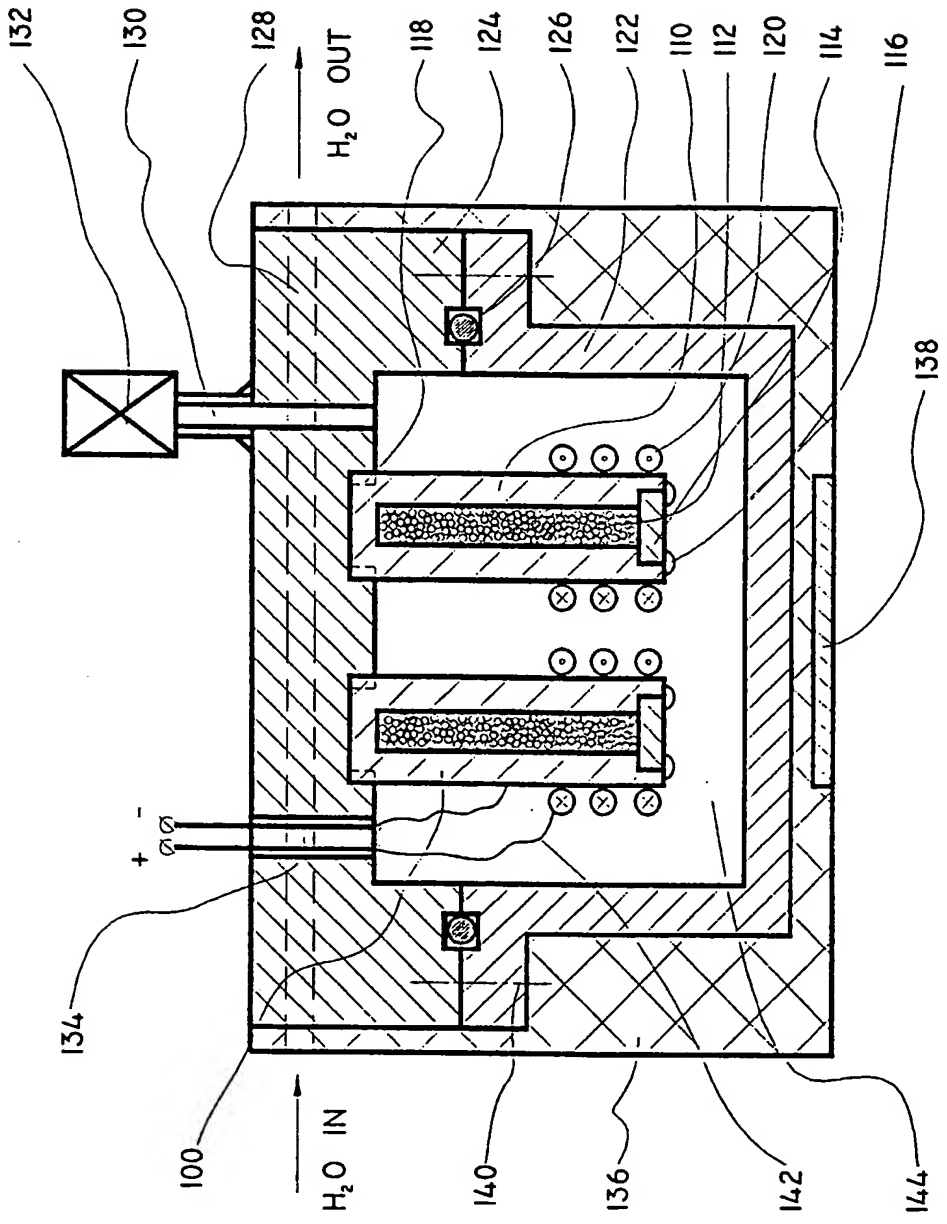
132
130
128
H_2O OUT
118
124
126
122
110
112
120
114
116
138
+
-
134
100
H_2O IN
140
136
142
144

FIG. 26

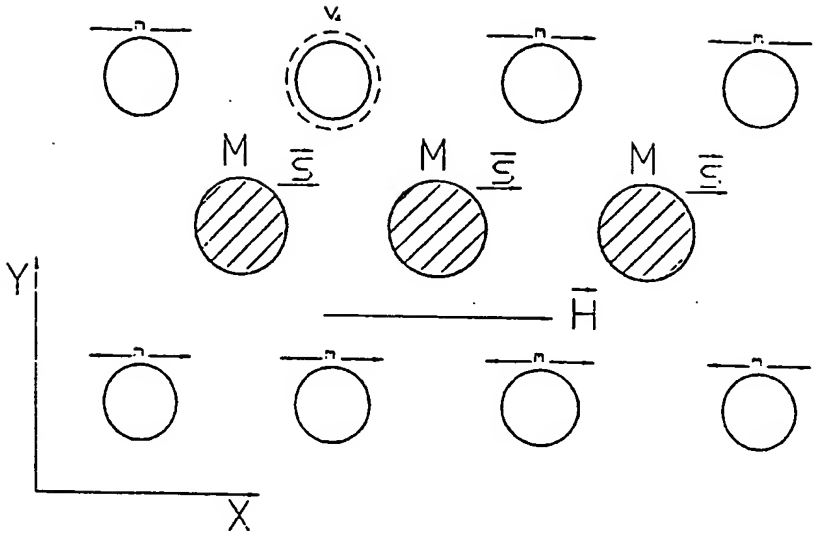

FIG. 27

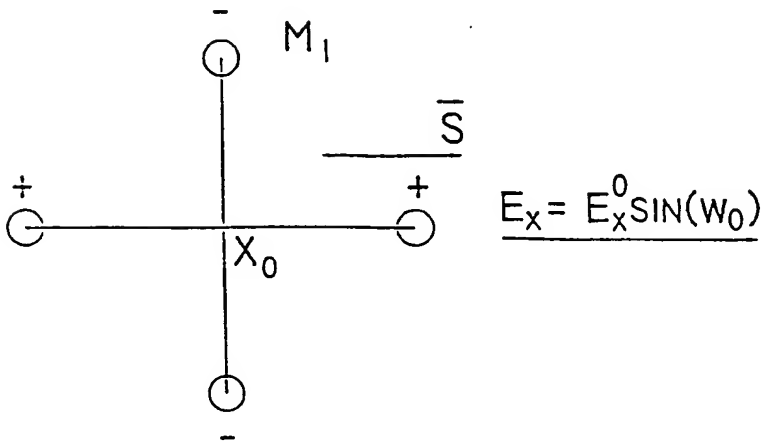

FIG. 28